


RESEARCH

Open Access



A proteomics analysis of 5xFAD mouse brain regions reveals the lysosome-associated protein *Arl8b* as a candidate biomarker for Alzheimer's disease

Annett Boeddrich¹, Christian Haenig¹, Nancy Neuendorf¹, Eric Blanc², Andranik Ivanov², Marieluise Kirchner³, Philipp Schleumann¹, Irem Bayraktaroglu¹, Matthias Richter⁴, Christine Mirjam Molenda⁴, Anje Sporbert⁴, Martina Zenkner¹, Sigrid Schnoegl¹, Christin Suenkel⁵, Luisa-Sophie Schneider⁶, Agnieszka Rybak-Wolf⁵, Bianca Kochnowsky⁶, Lauren M. Byrne⁷, Edward J. Wild^{7,8}, Jørgen E. Nielsen⁹, Gunnar Dittmar^{3,10}, Oliver Peters^{6,11}, Dieter Beule² and Erich E. Wanker^{1*} 

Abstract

Background Alzheimer's disease (AD) is characterized by the intra- and extracellular accumulation of amyloid- β (A β) peptides. How A β aggregates perturb the proteome in brains of patients and AD transgenic mouse models, remains largely unclear. State-of-the-art mass spectrometry (MS) methods can comprehensively detect proteomic alterations, providing relevant insights unobtainable with transcriptomics investigations. Analyses of the relationship between progressive A β aggregation and protein abundance changes in brains of 5xFAD transgenic mice have not been reported previously.

Methods We quantified progressive A β aggregation in hippocampus and cortex of 5xFAD mice and controls with immunohistochemistry and membrane filter assays. Protein changes in different mouse tissues were analyzed by MS-based proteomics using label-free quantification; resulting MS data were processed using an established pipeline. Results were contrasted with existing proteomic data sets from postmortem AD patient brains. Finally, abundance changes in the candidate marker *Arl8b* were validated in cerebrospinal fluid (CSF) from AD patients and controls using ELISAs.

Results Experiments revealed faster accumulation of A β 42 peptides in hippocampus than in cortex of 5xFAD mice, with more protein abundance changes in hippocampus, indicating that A β 42 aggregate deposition is associated with brain region-specific proteome perturbations. Generating time-resolved data sets, we defined A β aggregate-correlated and anticorrelated proteome changes, a fraction of which was conserved in postmortem AD patient brain tissue, suggesting that proteome changes in 5xFAD mice mimic disease-relevant changes in human AD. We detected a positive correlation between A β 42 aggregate deposition in the hippocampus of 5xFAD mice and the abundance of the lysosome-associated small GTPase *Arl8b*, which accumulated together with axonal lysosomal membranes

*Correspondence:

Erich E. Wanker
erich.w@mdc-berlin.de

Full list of author information is available at the end of the article



© The Author(s) 2023. **Open Access** This article is licensed under a Creative Commons Attribution 4.0 International License, which permits use, sharing, adaptation, distribution and reproduction in any medium or format, as long as you give appropriate credit to the original author(s) and the source, provide a link to the Creative Commons licence, and indicate if changes were made. The images or other third party material in this article are included in the article's Creative Commons licence, unless indicated otherwise in a credit line to the material. If material is not included in the article's Creative Commons licence and your intended use is not permitted by statutory regulation or exceeds the permitted use, you will need to obtain permission directly from the copyright holder. To view a copy of this licence, visit <http://creativecommons.org/licenses/by/4.0/>. The Creative Commons Public Domain Dedication waiver (<http://creativecommons.org/publicdomain/zero/1.0/>) applies to the data made available in this article, unless otherwise stated in a credit line to the data.

in close proximity of extracellular A β plaques in 5xFAD brains. Abnormal aggregation of Arl8b was observed in human AD brain tissue. Arl8b protein levels were significantly increased in CSF of AD patients.

Conclusions We report a comprehensive biochemical and proteomic investigation of hippocampal and cortical brain tissue derived from 5xFAD transgenic mice, providing a valuable resource to the neuroscientific community. We identified Arl8b, with significant abundance changes in 5xFAD and AD patient brains. Arl8b might enable the measurement of progressive lysosome accumulation in AD patients and have clinical utility as a candidate biomarker.

Keywords Proteomics, Alzheimer's disease, 5xFAD, Amyloid- β Amyloidogenesis, Aggregation, Arl8b, Biomarker

Background

Alzheimer's disease (AD) is the most common form of dementia in the elderly; its prevalence is growing rapidly in aging societies [1]. In 2050, ~150 million people worldwide are estimated to be affected by AD, imposing a substantial burden on patients and health care systems [1].

AD is a chronic neurodegenerative illness with a long preclinical phase (~20 years) and an average clinical duration of 8–10 years [2, 3]. Most patients with AD (>95%) have the sporadic form, which is characterized by late disease onset (80–90 years) and progressive neurodegeneration in wide areas of the cerebral cortex and the hippocampus [3, 4]. Sporadic AD is also often associated with the accumulation of amyloid- β (A β) peptides in intracellular deposits and extracellular plaques [5] as well as the aggregation of the microtubule protein tau, leading to the formation of neurofibrillary tangles (NFTs) in neurons [6]. A β peptides are derived by proteolytic cleavage of the amyloid precursor protein (APP) by γ - and β -secretases, which include presenilin 1 (PS1) and presenilin 2 (PS2) that are encoded by the genes *PSEN1* and *PSEN2*, respectively [7, 8].

The “amyloid cascade hypothesis” states that the release of A β peptides from APP and their self-assembly into amyloidogenic aggregates are the direct cause of dementia in AD patients [9, 10]. Thus, the formation of “proteopathic” A β assemblies is potentially at the root of AD and may drive all subsequent molecular pathogenic processes that eventually lead to the appearance of disease symptoms such as memory loss and progressive cognitive impairment. However, the linearity of the A β -driven disease cascade remains controversial. It provides no good explanation for the very long prodromal phase in AD as well as for the relatively weak correlation between the abundance of amyloid plaques in specific brain regions and the much later observed disease symptoms in sporadic AD patients [11].

A more direct causal link between A β production and disease development is established for familial AD (FAD), where causative mutations in *APP*, *PSEN1*, and *PSEN2* lead to early onset of AD (mean age of ~45 years) and the enhanced production of a 42-residue-long A β peptide

(A β 42) that is a major component of extracellular amyloid plaques in patient brains [12] and rapidly aggregates in cell-free assays and AD models [13]. Experimental evidence was obtained that imbalance between production and clearance of A β 42 and related A β peptides is a very early, even initiating event in AD [14]. This is also supported by the discovery of AD risk proteins such as ApoE4, SORL1, and PICALM that are all thought to play a specific functional role in A β clearance in AD brains [15–17]. Soluble A β 42 oligomers isolated directly from cortex of patients can dose-dependently decrease synaptic function and significantly impair memory of a learned behavior in healthy adult rats, representing further evidence for disease relevance of the polypeptide [18]. Finally, biomarker studies with FAD patients carrying *APP*, *PSEN1*, and *PSEN2* mutations have elucidated the pathogenic sequence of events in AD brains. In this context, it was demonstrated that the A β 42 levels in CSF start to decrease ~25 years before expected symptom onset [2]. This is then followed by the appearance of fibrillar PIB-reactive amyloid deposits (detected by PET studies), increased levels of tau in CSF and progressive brain atrophy roughly 15 years before expected symptom onset [2]. Thus, it seems adequate to speculate that progressively accumulating A β 42 peptides cause “aggregate” stress in FAD patient brains [19], which finally leads to progressive neurodegeneration and dementia.

The 5xFAD transgenic (tg) mouse model recapitulates major features of AD amyloid pathology [20, 21]. These mice express both human APP and PS1 with five FAD mutations in neurons, leading to overproduction of A β 42 peptides, which progressively accumulate in intraneuronal deposits and extracellular amyloid plaques [5] in mouse brains. Strikingly, A β 42 aggregation in 5xFAD mouse brains is accompanied by activated neuroinflammation, loss of synapse functions and neurodegeneration, which are all well-known pathobiological features of AD patient brains [20, 22–24]. In a recent proteomics study, convincing data were obtained that proteome changes in brains of 5xFAD tg mice and AD patients are cross-correlated [25], supporting the hypothesis that this disease model mimics key aspects of AD pathogenesis.

Here, we have investigated the impact of progressive A β 42 aggregation on the proteome in hippocampus and cortex of 5xFAD tg mice to elucidate the direct molecular consequences of A β 42-aggregate stress in AD mouse brains. We hypothesized that the proteome response to A β 42 aggregates might be distinct in hippocampus and cortex, because protein composition and abundance are significantly different in these brain regions [26]. Previous “OMICS” studies have shown changes in transcript and protein levels in brains of 5xFAD tg mice [20, 22–25, 27, 28]. However, a direct link between progressive A β 42 accumulation and proteome changes in specific disease-relevant brain regions such as hippocampus and cortex remains to be elucidated. Also, the concordance of proteome changes in 5xFAD and AD patient brains has previously not been assessed.

Here, we present experimental results indicating that progressive A β 42-mediated aggregate stress is associated with brain region-specific proteome changes in 5xFAD mouse brains. We observed that A β 42 aggregation was more pronounced in hippocampus than in cortex in AD mouse brains and that this phenomenon was also accompanied by a high number of proteins that changed in their abundance. Utilizing our data sets, we defined A β aggregate-correlated and anticorrelated proteome changes in 5xFAD brains, a fraction of which was also conserved in postmortem AD patient brains, suggesting that the observed proteome changes in mouse brains at least in part reflect the pathogenic process in patient brains. Furthermore, our investigations revealed that the small GTPase Arl8b, which controls lysosomal-related vesicle transport in neurons [29], strongly correlates with the progressive accumulation of A β 42 aggregates and is abnormally enriched in the vicinity of amyloid plaques in brains of 5xFAD tg mice. Finally, elevated levels of Arl8b were found in postmortem brain and CSF samples of AD patients, suggesting that this protein is of disease relevance and a candidate AD biomarker. The implications of our results for the development of protein biomarkers that potentially monitor the abnormal accumulation of lysosomes in response to A β aggregation in AD patient brains are discussed.

Methods

Antibodies

Commercially available antibodies applied in this study are shown in Additional file 1: Table S1. The concentrations of antibodies used for immunoblotting (IB), ELISA, and immunostaining (IS) of brain slices are described in the method sections below. Secondary Alexa Fluor-labelled anti-rat, anti-mouse, and anti-rabbit antibodies were used for immunostaining, while peroxidase labelled anti-rabbit and anti-mouse secondary antibodies

were used for immunoblotting. Alexa Fluor 594-labelled anti- β -Amyloid 1–16 (clone 6E10) antibody is a fluorophore-labelled primary antibody which was used for immunostaining of amyloid- β (A β). A labelling with a secondary antibody is not necessary in this case. Production and characterization of the mouse monoclonal antibody 352 applied for immunostaining was described previously [30]. This antibody specifically recognizes fibrillar A β 42 aggregates but not monomers in dot blot assays.

Analysis of CSF samples of AD and HD patients

AD ($n=38$) and control ($n=44$) CSF samples were obtained from patients at the Memory Clinic of Charité University Medicine Berlin. The characteristics of AD patients and controls and their CSF samples are listed in Additional file 1: Table S2. The procedures for CSF sample collection and treatment were described elsewhere [31, 32]. Briefly, CSF was collected in polypropylene tubes. Immediately after collection, the tubes were gently shaken and centrifuged ($2000\times g$; room temperature; 10 min). Supernatant was taken off, aliquoted, frozen in liquid nitrogen, and stored at -80°C . To quantify A β peptides in CSF, the Lumipulse[®] G β -Amyloid 1–42 and Lumipulse[®] G β -Amyloid 1–40 assays (Fujirebio Germany GmbH, Hannover, Germany) were used. For total (t)-tau and phosphorylated (p)-tau quantification, the Lumipulse[®] G Total Tau and Lumipulse[®] G p-Tau 181 assays (Fujirebio Germany GmbH, Hannover, Germany) were used, respectively. All measurements were carried out fully automatically on the LUMIPULSE[®] G600II instrument. Under these conditions, the following CSF biomarker values were rated as indicative of AD: A β (1–42) < 680 pg/ml, A β (1–42) / A β (1–40) ratio < 0.055, t-tau > 400 pg/ml and p-tau > 62 pg/ml (see Additional file 1: Table S2). Individuals who did not meet the abovementioned criteria were defined as control. The control group comprised CSF samples derived from subjective cognitive impairment patients, patients suffering from depression and healthy individuals. The AD group comprised CSF samples from AD patients with different grades of dementia. CSF samples from HD patients and controls were obtained from the Danish Dementia Research Centre [33] and the UCL Huntington’s Disease Centre, University College London, London, UK [34, 35].

Mouse model and breeding

5xFAD mice B6SJL-Tg(APP^SSwFLon, PSEN1*^{M146L}*L286V)⁶⁷⁹⁹Vas/Mmjax [21] overexpress two human AD-related proteins: the mutant human APP (695) protein with the Swedish (K670N), Florida (I716V) and the London (V717I) mutations and the human PS1 protein with the mutations M146L and L286V. 5xFAD mice

were backcrossed to C57BL/6NCrl mice for more than 10 generations (T. Willnow, MDC Berlin-Buch). For our experiment, female transgenic mice were mated to male wild-type mice. Resulting offspring were weaned at approximately 3 weeks of age; genotyping for the *APP* and *PSEN1* transgenes was performed by PCR with tissue biopsies [21]. Male mice of 2, 5, and 8 months were used for the experiments. Animal care was in accordance with the directive 2010/63/EU. The MDC has signed the Basel Declaration in 2012 and observes an internal animal welfare directive. Experimental procedures were approved by the local animal welfare authority in Berlin, Germany under license number TVV G0073/17. Mice were group-housed in cages with wooden bedding, environmental enrichment, and ad libitum food and water supply.

Mouse brain tissue processing

Mice, whose brains were used for immunohistochemistry analysis, were transcardially perfused with 25 ml 0.9% saline followed by 90 ml 4% paraformaldehyde in 0.1 M phosphate buffer pH 7.4 (PB) under deep anesthesia using pentobarbital (100–150 mg/kg). Brains were removed rapidly and post-fixed by immersion in 4% PFA in PB overnight. Then, the brains were cryoprotected by incubation in 20% sucrose in PB at 4 °C for 24 h followed by incubation in 30% sucrose in PB at 4 °C for 24 h. Brains were divided into hemispheres, frozen in isopentane and stored at –80 °C until cryosectioning. For all other analyses, mice were sacrificed by cervical dislocation. Brains were removed and washed in 1xPBS. Hippocampus and cortex were carefully dissected, frozen in liquid nitrogen, and stored at –80 °C until further use.

Preparation of brain homogenates

For preparation of mouse brain homogenates for membrane filter assays (MFAs) and gel analysis, ~80 mg brain was homogenized in 640 µl ice-cold 50 mM Tris pH 7.5 buffer containing protease inhibitors and Benzonase (0.25 U/µl) using the Precellys homogenizer (CK14 tubes, 5000 rpm, 14 s for cortex and CK14 tubes, 4500 rpm, 2 s for hippocampus). Then, 160 µl of a concentrated buffer solution containing 250 mM Tris pH 7.5, 750 mM NaCl, 0.5% SDS, 2% sodium deoxycholate, and 5% Triton were added to the homogenate and incubated for 30 min at 4 °C on a rotating wheel. The homogenate was transferred to a protein LoBind tube and centrifuged at 1.500×g for 20 min at 4 °C. Then, the supernatant was carefully removed and pipetted to a new tube. Protein concentration was determined using the Pierce BCA assay (Thermo Fisher Scientific, Waltham, MA, USA). Supernatant was stored at –80 °C until further use.

Human postmortem brain material

Human postmortem brain tissue samples from AD patients and controls were obtained from the Newcastle Brain Tissue Resource (NBTR), Newcastle University, UK. All samples originate from the temporal cortex. Characteristics of patients and Braak stage [36, 37] are summarized in Additional file 1: Table S2. Homogenates [38] of these brain samples were used for the Membrane Filter Assay (MFA) to determine the levels of Arl8a/b (Fig. 6a, b) and Arl8b (Additional file 2: Fig. S14a and b). To generate Fig. 6a and b, homogenates of cohort 1 were used for the MFA. To produce Additional file 2: Fig. S14a and b, homogenates of cohort 2 were used. Both cohorts differ in one AD patient.

Quantification of Aβ peptides with ELISA

To determine the amount of human Aβ40 and Aβ42 peptides in mouse brain homogenates, commercial ELISA kits (Thermo Fisher Scientific, Waltham, MA, USA: KHB3442, KHB3482) were used according to the manufacturer's instructions. Briefly, mouse brain material was weighed and homogenized using Precellys CK14 tubes as described above. To solubilize Aβ, homogenates were incubated with guanidine hydrochloride (final concentration 5 M) for 3.5 h with 800 rpm shaking at 22 °C. Then, samples were diluted and analyzed by ELISA.

Strategy of selecting the neuronal lysosome-associated protein Arl8b

Arl8b was selected for further analysis and characterization based on a rigorous selection process (Additional file 2: Fig. S12a and Additional file 3: Supplementary Excel File 8a) using the set of proteins detected in the hippocampus by quantitative mass spectrometry (MS). First, all proteins that were reliably measured in the majority of replicates, i.e., those that were “present” in the MS data, were extracted, resulting in 3571 proteins. Then, the statistical significance of the mean expression values of these proteins in transgenic mice versus wild-type mice was determined. Finally, only statistically significant proteins ($p_{adj} < 0.05$) were selected for further analyses, resulting in 699 DEPs (Fig. 2a). Next, we identified 400 DEPs that were also significantly altered in brains of Alzheimer's disease (AD) patients compared to controls (Fig. 4a, c, Additional file 2: Fig. S8 and Additional file 3: Supplementary Excel Files 4a–d and 5). Some of these DEPs, including Arl8b, emerged as top candidates, due to their significant increase in AD brains in three independent human proteomics data sets (J20, J22, and D22, Fig. 4a, c), indicating their potential role in AD. Furthermore, their expression was concordantly changed in both 5xFAD mouse and AD patient brains (Fig. 4c). In

total, 100 proteins were found to be altered concordantly. As part of these, the abundances of 9 proteins in 5xFAD mouse brains showed significant correlations with the time-dependent formation of A β aggregates, ranking them among the top 25 proteins with the highest effect size across all three time points (Fig. 3a). Among these 9 proteins, two proteins (Arl8b and Lamp1) were identified as neuronal endo-lysosomal proteins. Finally, Arl8b was selected as a widely novel and promising candidate for further investigation in the context of AD and due to its remarkably high significance of dysregulation at 8 months (Fig. 2a). Thus, Arl8b was defined by a stringent step-by-step selection process using both mouse and human proteomics data sets (Additional file 2: Fig. S12a and Additional file 3: Supplementary Excel File 8a).

Arl8b ELISA

Human Arl8b protein abundance was determined in CSF samples derived from AD and HD patients as well as control individuals. CSF was centrifuged at 2000 g for 10 min. The supernatant was carefully removed, diluted 1:18 in standard diluent delivered with the Arl8b ELISA kit (CUSABIO, CSB-EL002100HU). All steps were performed according to supplier protocols. Arl8b protein amounts in CSF samples were calculated using an Arl8b ELISA standard curve.

Western blot analysis

Protein extracts were boiled with NuPAGE 4 \times sample buffer containing 50 mM DTT for 5 min and then loaded onto NuPAGE Novex 4–12% Bis–Tris gels (Thermo Fisher Scientific). Electrophoresis was performed according to a standard protocol followed by transfer of proteins onto PVDF membrane (pore size 0.2 μ m, MerckMillipore) using a semidry blotting system (Power Blotter XL, Thermo Fisher Scientific) and a 2 \times NuPAGETM transfer buffer containing 10% methanol. Immunoblotting was performed using the method described previously [30]. The generated blots were blocked for 30 min with 3% skim milk (Sigma-Aldrich) in 1 \times PBS (13.7 mM NaCl, 0.27 mM KCl, 1 mM Na₂HPO₄, 0.2 mM KH₂PO₄, pH 7.4) containing 0.05% Tween 20 (PBS-T). Then, the membrane was incubated overnight with the primary antibody diluted in 3% skim milk PBS-T (6E10, 1:500; anti-Alpha-Tubulin (#T6074), 1:8000; anti-Alpha-Tubulin (SAB3501072), 1:2000; anti-Presenilin-1, 1:500; anti-Arl8b, 1:500; anti-LAMP1, 1:500; anti-Calnexin, 1:1000; anti-VDAC, 1:1000; anti-Golgin97, 1:750; anti-Flotillin, 1:1000, anti-NDUFB3, 1:1000). Subsequently, the membrane was washed three times for 10 min in PBS-T and incubated with the secondary peroxidase-conjugated anti-mouse or anti-rabbit antibody (1:2000) for 1 h at room temperature. The membrane was washed two

times for 5 min in PBS-T and two times for 10 min in PBS; immunoreactive protein was detected using Chemi-Glow (Biozym). Unless otherwise mentioned, chemiluminescence was measured with a FujiFilm LAS-3000 and images were quantified using the Aida image analysis software (Raytest).

Membrane filter assay

Mouse cortical and hippocampal brain homogenates were filtered through a cellulose acetate membrane with a pore size of 0.2 μ m (GE Healthcare Life Sciences, Munich, Germany). Per cavity of filtration unit, 10 μ g homogenate was filtered. Then, the membrane was washed with 1 \times PBS and blocked for 30 min with 3% skim milk in PBS-T. The protein aggregates retained on filter membranes were finally detected by antibody-based reactions as described for western blotting. The membrane filter assay procedure with human brain homogenates was described previously [38].

Cryosectioning

Frozen hemispheres of mouse brains were embedded in Tissue-Tek O.C.T. (Sakura) and sectioned using a CM3050 S Cryostat (Leica). Forty-micrometer-thick sections were collected in 24-well plates and stored in cryoprotectant solution (0.65 g NaH₂PO₄ \times H₂O, 2.8 g Na₂HPO₄ in 250 ml ddH₂O, pH 7.4 with 150 ml ethylene glycol, 125 ml glycerine) at 4 $^{\circ}$ C until further processing. Eight sections between bregma –1.4 mm to –3.6 mm [39] at equal distance from each other, determined by hemalum-eosin staining, were used for further analysis.

Hemalum-eosin staining

Free-floating sections were washed 2 \times 10 min with PBS, mounted on microscope slides and air dried. hemalum-eosin staining was carried out at room temperature. Sections were incubated with Mayer's hemalum (Roth) for 15 min followed by 10 min bluing in tap water. Sections were incubated in eosin (0.5% solution with a few drops of acetic acid) for 30 s followed by a wash in H₂O. Sections were subsequently treated with 50, 70, and 99% ethanol for 2 min/step and Xylol for 1 min. Sections were air-dried, mounted with Roti Histokitt (Roth), and covered with coverslips.

Immunostaining

Free-floating sections were transferred to a new 24-well plate and washed 2 \times 10 min with 1 \times PBS. Nonspecific binding was prevented by incubating the sections in blocking buffer (5% BSA, 0.3% Triton-X100 in 1 \times PBS) for 60 min at room temperature. Then, the sections were incubated with primary antibodies (352, 1:500; Lamp1, 1:200; Arl8b, 1:200; 6E10 Alexa 594, 1:200)

diluted in blocking buffer, overnight at 4 °C with gentle agitation. Sections were washed 3 times for 10 min with 1×PBS and incubated for 1 h at room temperature with the Alexa-fluorophor conjugated secondary antibody (1:1000) diluted in blocking buffer. Then, the sections were washed three times for 10 min with 1×PBS and stained with Hoechst (1:5000, Thermo Fisher Scientific) diluted in 1×PBS for 20 s. Sections were washed shortly in 1×PBS followed by ddH₂O and mounted onto glass slides (Superfrost-Plus) using fluorescence mounting medium (Dako Agilent). Since the 6E10 antibody is conjugated to Alexa Fluor 594 (Alexa Fluor® 594 anti- β -Amyloid, 1–16), incubation with a secondary antibody was not necessary. After incubation with Alexa 594 Fluor 6E10, brain sections were washed three times for 10 min with 1×PBS, mounted on slides, air dried shortly, and directly used for Thioflavin S staining.

Thioflavin S staining

Air dried sections were washed with PBS and incubated in 100, 95, and 80% EtOH for 2 min/step. Then, the sections were incubated in 1% Thioflavin S (MerckMillipore) solution for 15 min and washed with 50% EtOH for 1 min. Sections were briefly washed by 2 to 3 times dipping into H₂O and air dried shortly. One drop of fluorescence mounting medium (Dako Agilent) was added and sections were sealed with a coverslip (24×50 mm).

Microscopic imaging and image processing

Whole hemibrain sections were imaged using a Leica SP8 confocal laser scanning microscope (Leica Microsystems GmbH, Wetzlar). For quantification of plaques, Thioflavin S dye was excited with the 405-nm diode laser and

detected at 520 to 550 nm and Alexa Fluor 594-conjugated antibodies were excited with a 561-nm diode laser and detected at 610 to 700 nm. For correlation of Arl8b and 6E10 volumes, Alexa Fluor 594-conjugated antibodies were excited with a 561-nm laser and detected at 566 to 613 nm and Alexa Fluor 647 secondary antibodies staining Arl8b was excited with a 633-nm diode laser and detected at 640 to 700 nm. For detection, photomultiplier tubes (PMT) and Z-stack imaging were used. For quantification of plaques, eight sections per microscope slide were imaged in one workflow; images were acquired with a Plan Apo 20x/0.75 NA dry objective and the following settings: scan format 512×512 pixels, zoom 1x, pixel size of 1137 μ m, and a z-step of 0.685 μ m, scanner frequency of 600 Hz, pinhole at 1 Airy Unit, and bi-directional scan to increase speed. All images were acquired with identical settings.

To achieve data sets with higher resolution (Fig. 1f), images were acquired with a Plan Apo 63×/1.4 NA Oil Objective, a scan format of 2048×2048 pixels, scanner frequency of 100 Hz, line average of 2, and pinhole at 1 Airy Unit. The image sampling parameters were adjusted to the Nyquist-Shannon theorem (pixel size of 0.05 μ m and z-step of 0.15 μ m, zoom of 1.8). To improve signal-to-noise ratio for stitching of tiles, image restoration (deconvolution by CMLE algorithm) was done subsequent to imaging by using Huygens Professional Suite (Scientific Volume Imaging, SVI).

Plaque quantification

Plaque counts and plaque volumes were quantified using Imaris 9.2.1 surface function for surface detection. The detection threshold for each channel (6E10 or ThioS)

(See figure on next page.)

Fig. 1 Analysis of A β -peptide levels and -aggregation in brains of 5xFAD mice. **a** Hippocampal and cortical brain extracts of 2-, 5-, and 8-month-old AD ($n=5$) mice were used for A β 42 peptide ELISAs. As a control (Ctrl), a pool of wt mouse brain extracts was tested in parallel, which was produced by mixing equal protein amounts of tissue extracts derived from 5 different wt mice per age and tissue. The graph represents the mean \pm SD of five biological replicates of tg mice per age and tissue. Statistical analysis: Unpaired, two-tailed t -test between hippocampal and cortical samples of mice of the same age (**, $p=0.0054$). **b** Quantification of A β aggregates retained on filter membranes (Additional file 1: Fig. S2a) was performed using the Aida image analysis software. Per tissue and age, extracts of five different mice were analyzed. All data are expressed as mean \pm SD of five biological replicates. Statistical significance was assessed between hippocampal and cortical samples of mice with the same age using an unpaired, two-tailed t -test (**, $p=0.0016$). **c** Pearson correlation between A β 42 peptide levels determined by ELISA (blue line, right axis) and A β aggregates determined by MFA (purple line, left axis); hippocampal tissue samples were analyzed. The statistical significance of the association between the A β 42 peptide levels and A β aggregates was measured with a two-tailed t -test (*, $p=0.024$). **d** Plaque load was determined in hippocampus and cortex of 5xFAD mice at different ages ($n=5$ mice per age and tissue). Plaques were immunohistochemically stained with the antibody 6E10. Data represent mean \pm SD. The statistical significance was assessed between hippocampal and cortical tissues from the same age using an unpaired, two-tailed t -test (*, $p=0.0204$; ***, $p=0.0009$; ****, $p<0.0001$). **e** Plaque counts were determined in hippocampal and cortical tissues of 2-, 5-, and 8-month-old 5xFAD mice ($n=5$ per age and tissue) by antibody 6E10 and ThioS staining. Data represent mean \pm SD. The statistical significance was assessed with the antibody 6E10 (*, $p=0.0141$; ***, $p=0.0002$; ****, $p<0.0001$) and ThioS staining (ns; ***, $p=0.0003$; ****, $p<0.0001$) each for hippocampal and cortical tissues of mice with the same age using an unpaired, two-tailed t -test. **f** Immunofluorescence analysis of dense core (top row) and diffuse plaques (bottom row) in a brain slice of an 8-month-old 5xFAD mouse. Red indicates 6E10 immunoreactive material. Green indicates fibrillar A β material stained with ThioS. Yellow indicates merged signal. **g** Fractionation of hippocampal and cortical brain extracts derived from 8-month-old 5xFAD mice. Fractions from sucrose density gradient centrifugations of 10,000× g membrane pellets were analyzed by immunoblotting using antibodies detecting APP and amyloid- β (antibody 6E10), marker proteins of the endoplasmic reticulum (Calnexin), lipid rafts (Flotillin), the Golgi apparatus (Golgin97), lysosomes (Lamp1), and mitochondria (VDAC, NDUFB3). Equal exposure times per antibody for hippocampus and cortex are shown. Per fraction, equal volumes were loaded. From the solubilized pellet (P10,000× g), 5 μ g was loaded

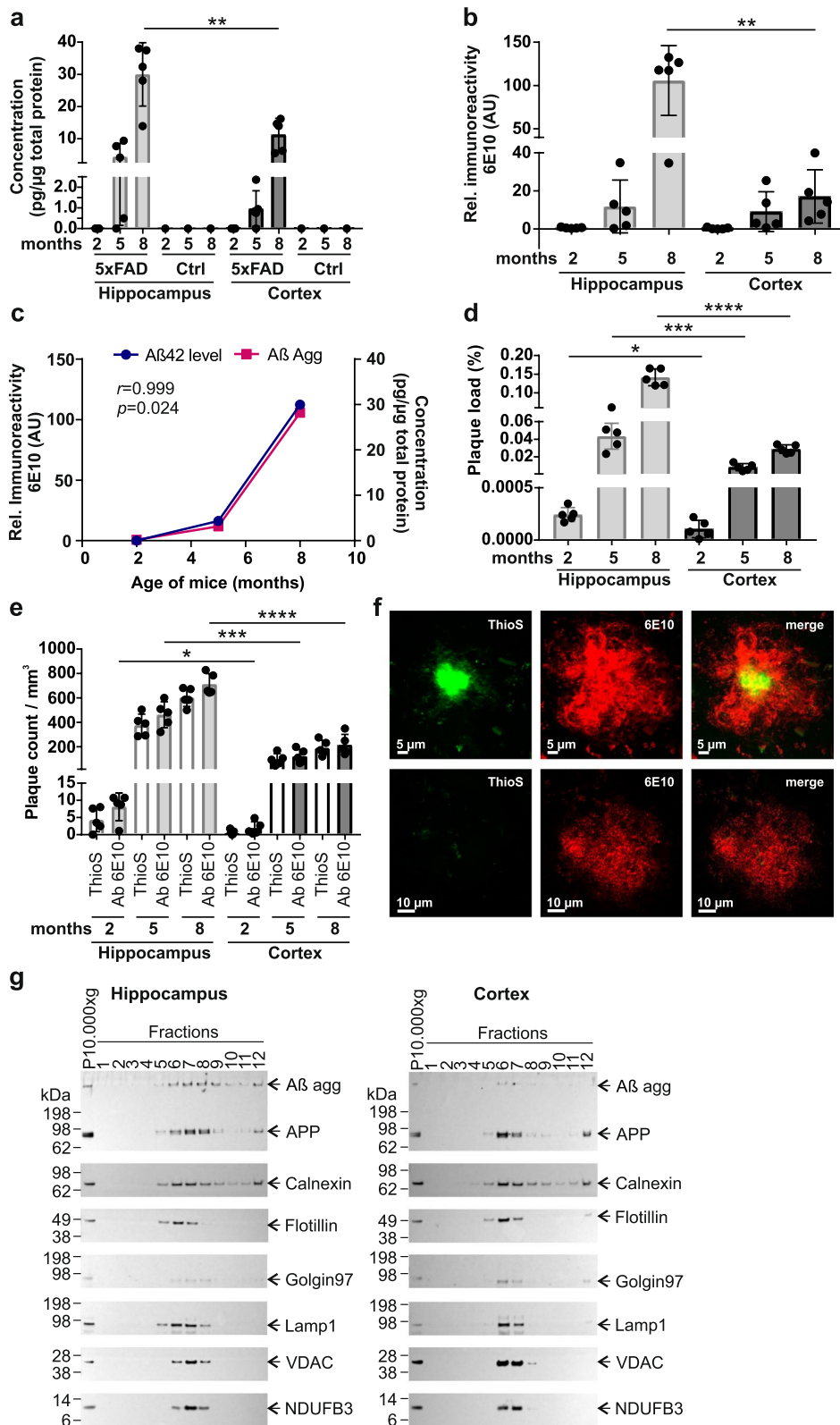


Fig. 1 (See legend on previous page.)

was set by hand and slightly adjusted within a range of a reference point to obtain values as constant as possible. Plaques smaller than $50 \mu\text{m}^3$ were excluded from quantification. The total area of hippocampus and cortex was measured in each section and normalized with $40\text{-}\mu\text{m}$ section thickness to determine their respective volume. Artifacts from staining, sectioning, or handling were excluded manually. Plaques were separately quantified per section in each region and the respective plaque volumes and plaque counts were determined. Based on these, the plaque load was calculated as the proportion of the hippocampal or cortical volume occupied by plaques: $\text{A}\beta \text{ Plaque Load (\%)} = (\text{Total Volume Plaques} / \text{Total Volume Region}) \times 100$. For quantification of Arl8b volume, Imaris 9.6 Software (Bitplane) was used. The detection threshold was set manually and slightly adjusted within the range of a reference point to maintain values as constant as possible.

Reverse transcription and quantitative real-time PCR

To purify RNA from hippocampus and cortex, the RNeasy Lipid Tissue kit (Qiagen) was used. DNA contamination was removed from purified RNA by using the RNase-Free DNase set (Qiagen). RNA concentration was determined by measuring the absorbance at 260 nm. Single-stranded cDNA from total RNA was synthesized using the High Capacity cDNA Reverse Transcription kit (Thermo Fisher Scientific). For real-time PCR of human APP, 10 ng cDNA was amplified with a TaqMan gene expression assay (Thermo Fisher Scientific: Hs00169098_m1) and TaqMan Gene Expression Master Mix (Thermo Fisher Scientific) in a total volume of 10 μl . For normalization of data, an endogenous mouse EIF-4H (Mm00504282_m1) FAM/MGB labelled probe (Thermo Fisher Scientific) was used. For real-time PCR of human *PSENI*, 10 ng cDNA was amplified with a TaqMan gene expression assay (Thermo Fisher Scientific: Hs00997789_m1) and TaqMan Gene Expression Master Mix (Thermo Fisher Scientific) in a total volume of 10 μl . For normalization of data, an endogenous mouse *GAPDH* (Mm99999915_g1) FAM/MGB labelled probe (Thermo Fisher Scientific) was used. Real-time PCR was performed using the ViiA 7 real-time PCR system (Applied Biosystems). Samples were measured in triplicates. Quantification was performed using the ΔCt method and the QuantStudio real-time PCR Software v1.3.

Preparation of mouse brain samples for mass spectrometric analysis

Mouse brain material was weighed and homogenized in lysis buffer (6 M guanidinium chloride, 100 mM Tris pH 8.5, 10 mM TCEP, 40 mM CAA, 20% weight/volume), heated for 5 min at 95°C , cooled on ice for 15 min,

followed by sonication. After centrifugation for 30 min at $3500 g$ (4°C), the supernatant (soluble protein fraction) was transferred to a fresh tube and mixed with 4 volumes of ice-cold acetone, followed by incubation over night at -20°C . Samples were centrifuged for 15 min at $12,000 g$ (4°C), and the resulting protein pellets were washed with ice-cold 80% acetone, air dried, and resuspended in digestion buffer (6 M urea, 2 M thiourea, 100 mM Hepes, pH 8). The samples were sonicated using a Branson probe SonifierTM (output 3–4, 50% duty cycle, 4×30 s). Protein concentration was determined using a Bradford assay (BioRad). Samples were stored at -80°C until use. 50 micrograms of protein per sample were used for tryptic digestion. First, Endopeptidase Lys-C (Wako, Japan) was added in a protein:enzyme ratio of 50:1 and incubated for 4 h at room temperature. After dilution of the sample with 4 volumes 50 mM ammonium bicarbonate (pH 8.0), sequencing grade modified trypsin (Promega) was added (protein:enzyme ratio 100:1) and digested overnight at room temperature. Trypsin and Lys-C activity was quenched by acidification with TFA to pH ~ 2 . Peptides were cleaned up using the StageTip protocol [40].

Mass spectrometric analyses

For mass spectrometric analyses, peptide samples (2 μg per measurement) were separated by reversed-phase chromatography using the Eksigent NanoLC 400 system (Sciex) on in-house manufactured 20-cm fritless silica microcolumns with an inner diameter of $75 \mu\text{m}$, packed with $3 \mu\text{m}$ ReproSil-Pur C18-AQ beads. A 8–60% acetonitrile gradient (224 min) at a nano-flow rate of 250 nl/min was applied. Eluting peptides were directly ionized by electrospray ionization and analyzed on a Thermo Orbitrap Fusion (Q-OT-qIT, Thermo). Survey scans of peptide precursors from 300 to 1500 m/z were performed at 120 K resolution with a 2×10^5 ion count target. Tandem MS was performed by isolation at 1.6 m/z with the quadrupole, HCD fragmentation with normalized collision energy of 30, and rapid scan MS analysis in the ion trap. The MS² ion count target was set to 2×10^3 and the maximum injection time was 300 ms. Only precursors with charge state 2–7 were sampled for MS². The dynamic exclusion duration was set to 60 s with a 10 ppm tolerance around the selected precursor and its isotopes. The instrument was run in top speed mode with 3-s cycles, meaning the instrument would continuously perform MS² events until the list of nonexcluded precursors diminishes to zero or 3 s. For all samples, 2 technical replicates were performed (for 5 months hippocampus, 3 technical replicates were measured).

Analysis of mass spectrometric data

Data were analyzed by MaxQuant software (v1.5.1.2). The internal Andromeda search engine was used to search MS² spectra against a decoy human UniProt database (MOUSE.2014–10) containing forward and reverse sequences. The search included variable modifications of methionine oxidation and N-terminal acetylation, deamidation (NQ), and fixed modification of carbamidomethyl cysteine. Minimal peptide length was set to seven amino acids and a maximum of two missed cleavages was allowed. The FDR was set to 1% for peptide and protein identifications. The integrated LFQ quantitation algorithm was applied. Unique and razor peptides were considered for quantification with a minimum ratio count of 1. Retention times were recalibrated based on the built-in nonlinear time-rescaling algorithm. MS² identifications were transferred between runs with the “Match between runs” option, in which the maximal retention time window was set to 2 min.

Quantification of differential protein abundance

The LFQ intensities obtained from MaxQuant were batch-corrected separately for cortex and hippocampus data using the Combat [39] algorithm on log₁₀ LFQ intensities. No missing intensity values imputation was performed. Instead, we adopted a conservative approach, keeping for analysis only proteins with reliable intensity

measures across the majority of conditions. In a first selection step, we grouped the data by tissue, age, and genotype. When a protein had missing intensity values in half of the samples or more for each individual condition, it was deemed unreliable and was excluded. The number of proteins reliably measured in the cortex ranged from 3602 to 3752 (median 3651), as 4915 proteins were quantified in this dataset, i.e., 1163 and 1313 (median 1264) proteins were discarded. In the hippocampus dataset, 5069 proteins were quantified and between 3434 and 3620 (median 3502) proteins were deemed reliably measured according to the described threshold. In the next step, we ensured that protein intensities were reliably measured in both 5xFAD and control samples collected in the same tissue and at the same age. The number of proteins reliably measured in both genotypes are 3613 (2 months), 3476 (5 months), and 3524 (8 months) in cortex, and 3337 (2 months), 3471 (5 months), and 3248 (8 months) in hippocampus. These proteins were used for the analysis of the transgene effect when it was restricted to samples collected at the same age and in the same tissue. In total, we identified 699 differentially expressed proteins defined through the “pairwise model” (Fig. 2b, Additional file 3: Supplementary Excel File 1a, b) that are significantly dysregulated at 2, 5, or 8 months in at least one tissue. DEPs across all time points (DE.cortex.Age2, DE.cortex.Age5 and DE.cortex.Age8; DE.hippo.Age2,

(See figure on next page.)

Fig. 2 Differential expression analysis of proteins in brains of 5xFAD mice. **a** Volcano plots depicting the protein expression logarithmic fold-changes (log₁₀ fold-change, x-axis) and the adjusted *p*-values (−log₁₀ *p*-value, y-axis). Differentially Expressed proteins across all time points (Age 2, 5, and 8) in cortex and hippocampus were analyzed (DE.cortex.Age2, DE.cortex.Age5 and DE.cortex.Age8; DE.hippo.Age2, DE.hippo.Age5 and DE.hippo.Age8). All proteins highlighted in blue have significantly altered expression. The candidate AD biomarker Arl8b, marked in red, is significantly upregulated in hippocampus. Gene names for potential proteins of interest with highly significant fold-changes are indicated. Proteins not significantly changed in their abundance are highlighted in gray. Significance was determined using a two-tailed *t*-test and a Benjamini–Hochberg False Discovery Rate (FDR) set to 5%. **b** Numbers of differentially expressed proteins obtained by comparing the protein expression measurements of 5xFAD mice at different ages with their corresponding, age-matched, wild-type controls in cortex and hippocampus. The identifiers of the amounts of proteins analyzed were denoted analogously as in panel **a**. Bars indicate the numbers of significant down- (blue) and upregulated (red) proteins. **c** Numbers of proteins significantly differentially regulated. A2TC (Age 2, Tissue Cortex), A5TC and A8TC label the numbers of proteins for which the transgene effect is significant in cortex, at 2, 5, and 8 months, respectively. Proteins more abundant in 5xFAD mice are shown in red, while proteins more abundant in wild-type mice are shown in blue. A2TH (Age 2, Tissue Hippocampus), A5TH, and A8TH label the same comparison in hippocampus. A52TC (Age 5 vs 2, Tissue Cortex), A85TC and A82TC refer to the numbers of proteins for which the transgene effect is significantly different at two time points (5 vs 2, 8 vs 5, and 8 vs 2 months) in cortex. The numbers of proteins which increase in abundance with age are shown in red, while the numbers of proteins that decrease with age are shown in blue. The corresponding labelling for the hippocampus samples are A52TH (Age 5 vs 2, Tissue Hippocampus), A85TH and A82TH. Finally, A2THC (Age 2, Tissue Hippocampus vs Cortex), A5THC and A8THC report the numbers of proteins for which the transgene effect is significantly different in cortex and hippocampus at 2, 5, and 8 months, respectively. Higher hippocampus abundance is shown in red on the right, and higher cortex abundance in blue on the left. The underlying data are available as Additional file 3: Supplementary Excel File 1c. **d–f** Venn diagrams showing the numbers of total (**d**), downregulated (**e**), and upregulated (**f**) proteins in cortex and hippocampus, including only significantly differentially expressed proteins (DEPs). The amounts of DEPs were denoted analogously to panel **c** but were combined across all time points (months 2, 5, and 8); the combination of DEPs is indicated by the x (e.g., AxTC). **g** Correlation analysis of DEPs for A2TC, A8TC, A2TH, A5TH, and A8TH. The degree of correlation was assessed by Spearman correlation coefficients (*r*_s) and corresponding FDR-adjusted *p*-values (**, *p* < 0.01; ***, *p* < 0.001). Crosses indicate no correlation. The colors denote the values of the Spearman correlation coefficients. **h** Example Spearman inverse correlation of A2TC versus A8TC also shown in panel **g**. **i** Time-dependent changes in the abundance of 8 mitochondrial proteins and transcripts (**j**) that play a key role in oxidative phosphorylation and ATP production. The temporal changes of the LFCs across all ages (2, 5, and 8 months) in cortex (orange) and hippocampus (blue) are shown. The statistical significance of the differentially expressed proteins and transcripts was measured with a two-tailed *t*-test, adjusted by the Benjamini–Hochberg multiple testing correction (*, *p* < 0.05, **, *p* < 0.01; ***, *p* < 0.001). All analyses are based on mean values of measured intensities from five biological replicates of tg mice per age and tissue (*n* = 5)

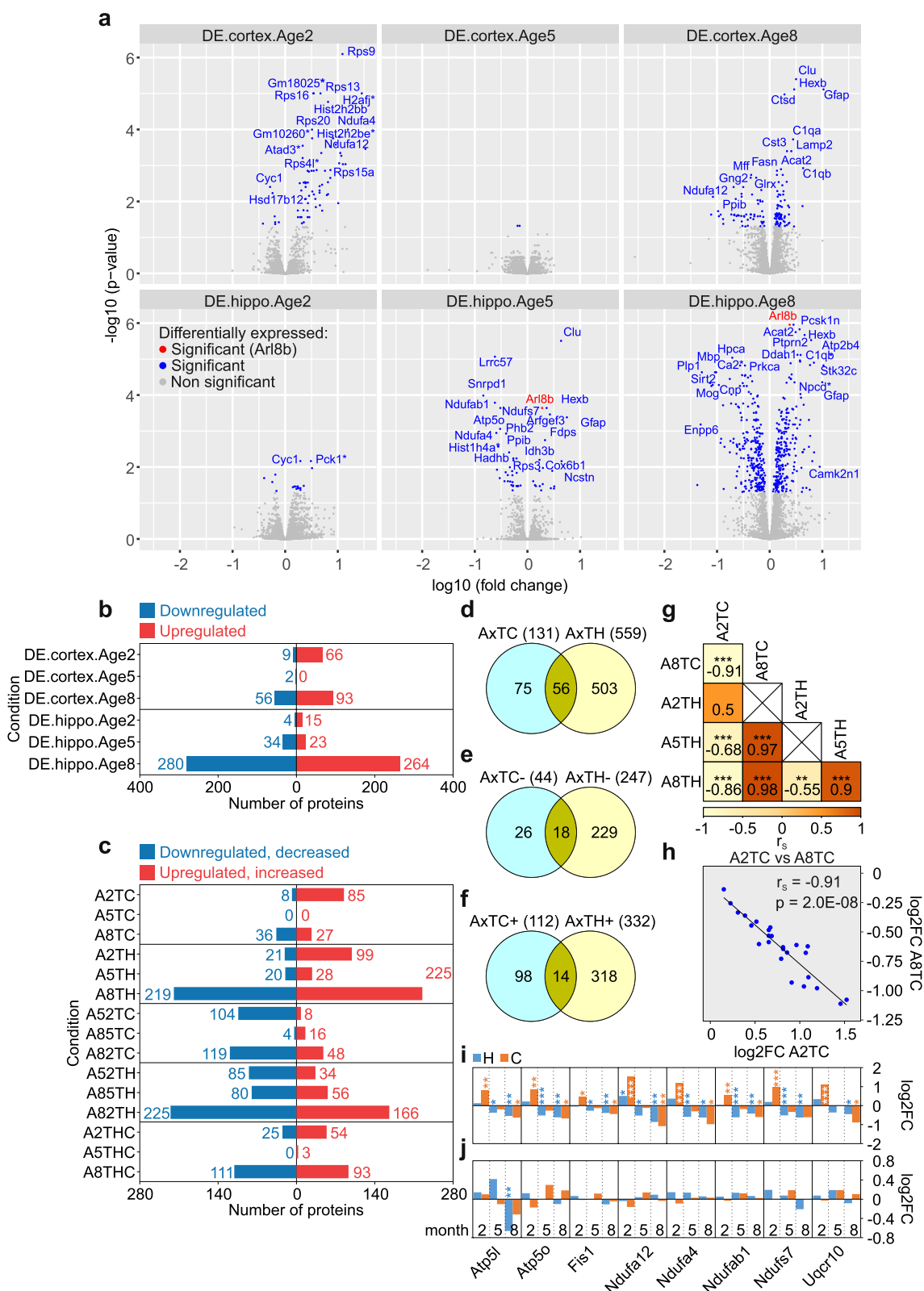


Fig. 2 (See legend on previous page.)

DE.hippo.Age5 and DE.hippo.Age8) are presented as volcano plots (Fig. 2a) that were generated with the ggplot2 package in R v.4.2.0. The volcano plots show the protein expression logarithmic fold-changes (\log_{10} FC; x -axis) and the adjusted p -values ($-\log_{10}$ p -value; y -axis). However, these pairwise models do not allow comparisons of the transgene effect across ages or tissues.

For this reason, we have created a set of proteins that are reliably measured in all conditions, suitable for all comparisons of transgene effects. For this set, we demanded that the proteins identified in the previous step should be reliably measured in each tissue, in all time points. These requirements reduced the numbers to 3281 and 3047 proteins for the cortex and hippocampus, respectively. Finally, only proteins common to the filtered cortex and hippocampus datasets were included in the statistical model. Please note that the Andromeda assignment of peptides to proteins may differ between cortex and hippocampus datasets. As a result, some peptides are attributed to several proteins and in rare cases this may lead to ambiguous mapping of proteins. Therefore, we discarded any many-to-many relationships between cortex and hippocampus proteins. Eventually, 2761 reliably measured proteins common to both tissues were used in the final full statistical model for differential protein analysis. While our filtering discards many proteins, it allows the statistical estimation of transgene effect differences between conditions. In total, we identified 637 differentially expressed proteins defined through the “full model” (Fig. 2c, Additional file 3: Supplementary Excel File 1c) that are significantly dysregulated at 2, 5, or 8 months in at least one tissue (A2TC, A5TC or A8TC; A2TH, A5TH or A8TH).

To estimate the transgene effect, we analyzed differential intensities on a \log_{10} scale. Differential protein

abundance between wild-type and 5xFAD animals is estimated separately for each age group and in each tissue, using empirical Bayes statistics implemented in limma [40]. Replicated measures on the same animal were taken into account using the “duplicateCorrelation” procedure in limma. The differences in transgene effect between tissues or time points were obtained using contrasts to take the interaction effect into account. The Benjamini–Hochberg False Discovery Rate [41] was computed separately for each contrast. Proteins were considered differentially expressed when their FDR was below 0.05. To make sure that the aggregation of data from very different conditions does not distort the results obtained from the model, we compared transgene effects obtained using the full model to those obtained from pairwise models in each condition separately. Pearson correlation between t statistics estimated from the full model and the pairwise models are between 0.942 and 0.977 (median 0.955). This suggests that including data from different tissues does not have a strong influence on the transgene effect modelling.

Generating Venn diagrams to visualize overlaps in protein expression datasets of 5xFAD mice and human AD patient brains

Venn diagrams (Figs. 2d–f, 3e, 4a, Additional file 2: Fig. S10c) were generated using Venny 2.1.0 (<https://bioinfogp.cnb.csic.es/tools/venny/index.html>). They were used to determine the number of overlapping gene symbols. The Venn diagrams in Fig. 2d–f depict the number of differentially expressed proteins (DEPs) in cortex or hippocampus defined through the “full model” (Additional file 3: Supplementary Excel File 1c). The amounts of DEPs were combined across all time points (months 2, 5, and 8) that are indicated by

(See figure on next page.)

Fig. 3 Identification of $A\beta$ -correlated and anticorrelated protein alterations in 5xFAD brains. **a** Numbers of proteins that correlate (corr, in red) or anticorrelate (acorr, in blue) with $A\beta$ aggregates in hippocampus and cortex and are differentially expressed at 2 (DE.cortex.Age2, DE.hippo.Age2), 5 (DE.cortex.Age5, DE.hippo.Age5), or 8 (DE.cortex.Age8, DE.hippo.Age8) months. The identifiers were denoted analogously as in Fig. 2a. The degree of correlation was assessed by Pearson correlation and corresponding FDR-adjusted p -values. **b** Volcano plots depicting the protein expression logarithmic fold-changes (\log_{10} fold-change, x -axis) and the adjusted p -values ($-\log_{10}$ p -value, y -axis) across all time points (age 2, 5, and 8 months) for DEPs that correlate (corr) or anticorrelate (acorr) with $A\beta$ aggregates in hippocampus (h) and cortex (c). All proteins highlighted in blue are expressed significantly differently. The $A\beta$ -correlating AD biomarker candidate Arl8b is marked in red. Proteins of interest with highly significant fold-changes are indicated with gene names. Proteins not significantly changed are highlighted in gray. Significance was determined using a two-tailed t -test and a Benjamini–Hochberg False Discovery Rate (FDR) set to 5%. **c, d** Changes of *APOE* transcript (**c**) and protein (**d**) levels in hippocampus (H) and cortex (C) of 2-, 5-, and 8-month-old 5xFAD mice. LFC, \log_2 fold-change. **e** Number of differentially expressed genes (DEGs, light red) that overlap (purple) with $A\beta$ aggregate-correlated (corr) and anticorrelated (acorr) DEPs (light blue). **f** Time-dependent changes in the abundance of 9 correlating or anticorrelating molecules; both protein (top) and transcript (bottom) level changes are shown. The temporal changes of the t -scores across all ages (2, 5, and 8 months) in cortex (orange) and hippocampus (blue) are illustrated. The statistical significance of differentially expressed proteins and transcripts was measured with a two-tailed t -test, adjusted by the Benjamini–Hochberg multiple testing correction (*, $p < 0.05$; **, $p < 0.01$; ***, $p < 0.001$). **g** Ingenuity pathway analysis (IPA) for the correlating or anticorrelating molecules that are changed both at the protein and transcript level as shown in panels **e** and **f**. The statistical significance of the association between the DEPs and the canonical pathways was measured with right-tailed Fisher’s exact test to calculate the p -values, adjusted by the Benjamini–Hochberg multiple testing correction. All analyses are based on mean values of measured intensities from five biological replicates of tg mice per age and tissue ($n = 5$)

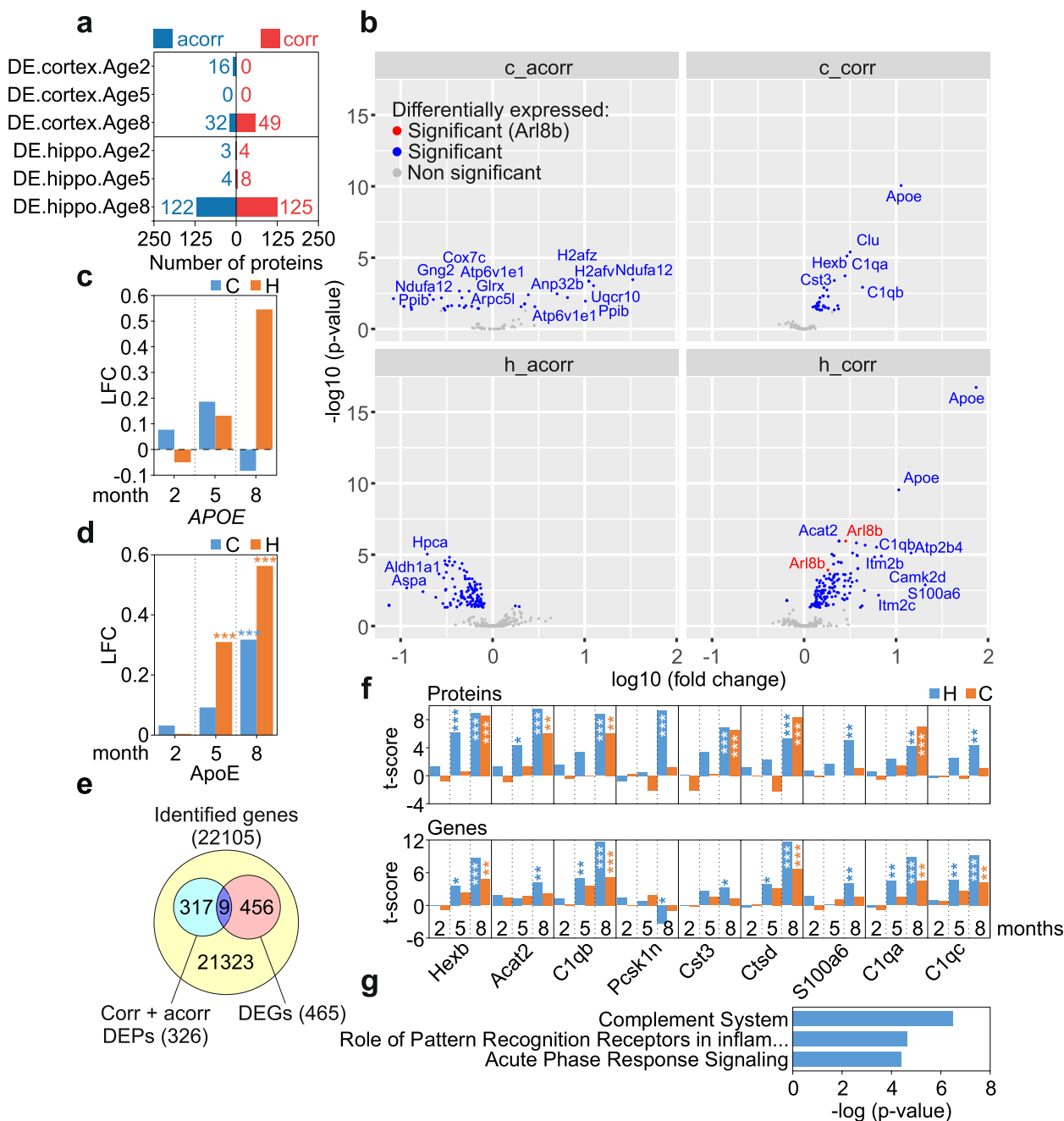


Fig. 3 (See legend on previous page.)

the “x” in, e.g., AxTC. Figure 3e shows the number of differentially expressed genes (DEGs; Additional file 3: Supplementary Excel File 3) that overlap with A β aggregate-correlated (corr) and anticorrelated (acorr) DEPs (Additional file 3: Supplementary Excel File 2). Figure 4a depicts the overlaps (Additional file 2: Fig. S8 and Additional file 3: Supplementary Excel File 6) of differentially expressed proteins (DEPs) in brains

of 5xFAD mice from the “pairwise model” (Additional file 3: Supplementary Excel File 1a, b) and postmortem brains of AD patients from Johnson 2020 [41] (Additional file 3: Supplementary Excel File 5a), Johnson 2022 [42] (Additional file 3: Supplementary Excel File 5b) and Drummond 2022 [43] (Additional file 3: Supplementary Excel File 5d). In Additional file 2: Fig. S10c, the overlap of DEPs that are concordantly up- or

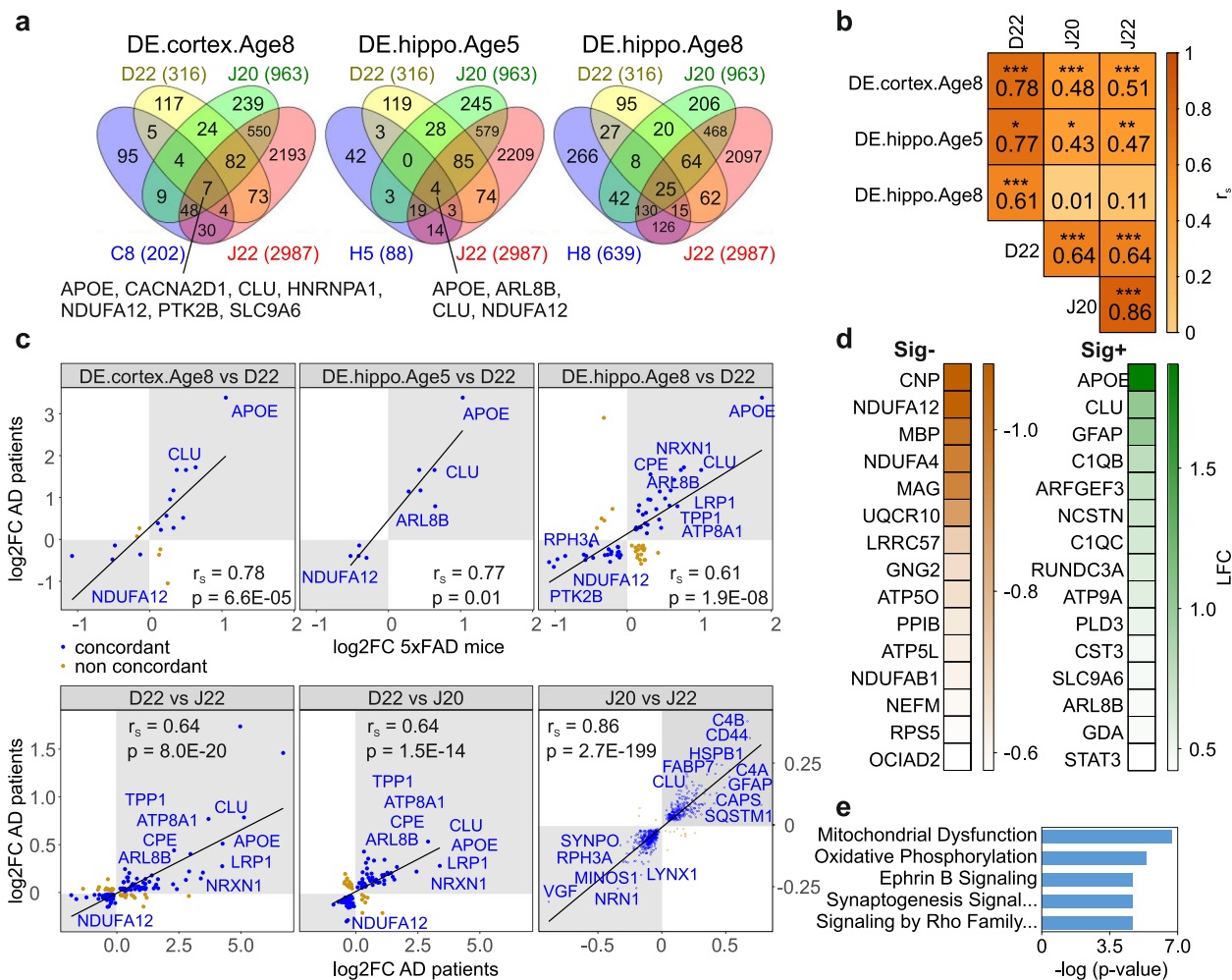


Fig. 4 Analysis of dysregulated proteins of 5xFAD brains and postmortem brains of AD patients. **a** Investigation of the overlap of DEPs in brains of 5xFAD mice and postmortem AD patients. Protein changes in cortical and hippocampal tissues of 8- and 5-month-old mice (DE.cortex.Age8; DE.hippo.Age5; DE.hippo.Age8) that contain A β aggregates (Fig. 1d) were compared with patient protein measurements. The amounts of DEPs are denoted analogously to Fig. 2a or have been abbreviated (C8, H5, H8). The human AD data were obtained from Drummond 2022 (D22, [43]), Johnson 2020 (J20, [41]), and Johnson 2022 (J22, [42]). The total numbers of DEPs in each dataset are indicated in brackets. In DE.cortex.Age8 and DE.hippo.Age5, the proteins present in all four data sets are depicted with gene names. **b** Correlation analyses of DEPs from cortical tissues of 8-month-old mice (DE.cortex.Age8) and DEPs from hippocampal tissues of 5- (DE.hippo.Age5) and 8-month-old mice (DE.hippo.Age8) with human AD patient data from Drummond 2022, Johnson 2020 and Johnson 2022 (as indicated in panel a) were performed. The degree of correlation was assessed by Spearman correlation coefficients (r_s) and corresponding FDR-adjusted p -values (*, $p < 0.05$; **, $p < 0.01$; ***, $p < 0.001$). Colors denote the values of the Spearman correlation coefficients. **c** Example Spearman correlations and concordance representations of dysregulated proteins from 5xFAD mice (DE.cortex.Age8, DE.hippo.Age5, and DE.hippo.Age8) versus human AD patient data from Drummond 2022 along with human AD data against each other (D22 vs J22, D22 vs J20, J20 vs J22) are shown. The identifiers are denoted analogously to Figs. 2a and 4a. Proteins concordantly up- or downregulated in 5xFAD mice and human AD patient brains are shown in gray quadrants and marked in blue. Proteins of interest with highly significant fold-changes are indicated with gene names. Correlating but non-concordant proteins are marked in brown. **d** Generation of signatures for proteins concordantly dysregulated in 5xFAD mice and human AD patient brains. The heatmaps show the 15 most down (Sig-, left) or upregulated (Sig+, right) proteins. Colors denote the values of the log₂ fold-changes. **e** Ingenuity pathway analysis (IPA) for the complete set of concordantly dysregulated proteins. The statistical significance of the association between the DEPs and the canonical pathways was measured with a right-tailed Fisher’s exact test to calculate p -values, adjusted by the Benjamini–Hochberg multiple testing correction. All analyses are based on mean values of measured intensities from five biological replicates of tg mice per age and tissue ($n = 5$)

downregulated in the hippocampus or cortex of 5xFAD mice, AD brains, and AsymAD patient brains is shown. The conc_AD dataset includes all DEPs concordantly

up- or downregulated in the hippocampus or cortex of both 5xFAD and AD patients, while conc_AsymAD includes those in 5xFAD and AsymAD patients.

RNA extraction and sequencing

The brain tissue was homogenized in TRIzol[®] Reagent (Ambion) using a Precellys homogenizer (Bertin Technologies) and extracted according to the TRIzol[®] Reagent protocol, with an additional phenol/chloroform purification step and the final isopropanol precipitation. For the total RNA sequencing, we used 1000 ng of total RNA; rRNA was depleted using an RNase H-based protocol. We mixed total RNA with 1 µg of a DNA oligonucleotide pool comprising a 50-nt-long oligonucleotide mix covering the reverse complement of the entire length of each human rRNA (28S rRNA, 18S rRNA, 16S rRNA, 5.8S rRNA, 5S rRNA, 12S rRNA), incubated with 1U of RNase H (Hybridase Thermostable RNase H, Epicentre), purified using RNA Cleanup XP beads (Agencourt), DNase treated using TURBO DNase rigorous treatment protocol (Thermo Fisher Scientific), and purified again with RNA Cleanup XP beads. We fragmented the rRNA-depleted RNA samples and processed them into strand-specific cDNA libraries using TruSeq Stranded Total LT Sample Prep Kit (Illumina) and then sequenced them on NextSeq 500, High Output Kit, 1 × 150 cycles.

Quantification of differential gene abundance

RNA-seq reads were mapped to the mouse GRCm38.p4 genome with STAR [44] (version 2.4.2.a). Reads were assigned to genes with featureCounts (version 1.4.6-p5) using the following parameters: -t exon -g gene_id, and with Genecode gcm38.p4-vM6 gtf reference [45]. The differential expression analysis was carried out with DESeq2 [46] (version 1.12.4) using default parameters.

Mapping of gene identifiers

The joint analysis of proteomics and transcriptomics data was done on genes. The LFQ intensity, the differential protein abundance, and associated statistical quantities were attributed to a gene by the following process: first, each protein identifier produced by the MaxQuant analysis software was assigned to an MGI gene identifier. This was done by matching the MaxQuant protein identifier with GenBank, UniProt, and TrEMBL protein ids obtained from MGI maker association files [47] downloaded in August 2017. This mapping provided connections between the initial protein identifier to NCBI & ENSEMBL gene identifiers. For protein ids unknown in MGD, direct queries to the UniProt database were made, and ENSEMBL biomart [48] was used to link the UniProt output to ENSEMBL & NCBI gene ids.

Orthologous gene mapping between mouse and human

To determine orthologs between mouse and human, we utilized the “orthogene” package in R, which is a reliable and commonly used tool for converting gene symbols or

Ensembl IDs into their corresponding orthologous gene symbols or Ensembl IDs in other species. The package employs the HomoloGene database (<https://www.ncbi.nlm.nih.gov/homologene/>) that provides curated orthology relationships among genes in various organisms. In our study, we primarily used gene symbols that were validated and, if needed, corrected prior to analysis. These gene symbols were converted from mouse to human and vice versa, with orthologous genes ideally mapped in a one-to-one ratio. The results from both translations were combined to minimize any biases in the data analysis, which could arise due to the consideration of different translation ratios (e.g., one-to-many) or inclusion of only one direction of translation, and to obtain an accurate representation of the overlaps.

Correlation analysis methods

To evaluate the relationship between the abundance changes of the differentially expressed proteins (DEPs) and the progressive Aβ aggregate formation in cortex and hippocampus of 5xFAD brains, we used the Pearson correlation coefficient r . We examined how the abundance changes of all 699 DEPs (Fig. 2a, b, Additional file 3: Supplementary Excel File 1a, b) are correlated or anticorrelated with the time-dependent accumulation of Aβ aggregates by associating the LFCs of the measured intensities of the DEPs with the abundance changes of Aβ aggregates across all ages (months 2, 5, and 8). Four different Aβ datasets were used: amounts of Aβ aggregates determined by MFA (Fig. 1b), Aβ plaque load (Fig. 1d), Aβ plaque counts determined by 6E10 antibody and ThioS staining (Fig. 1e). Each dataset consists of three data points, which are mean values of measured intensities from 5 biological replicates per age. For the correlation analysis, we examined the relationship between the three data points of the DEPs and the Aβ data sets separately for cortex and hippocampus. As a result, only DEPs with changes that correlate ($0 < r < 1$) or anticorrelate ($0 > r > -1$) significantly ($p_{\text{corr}} < 0.05$) with at least one of the mentioned Aβ datasets were considered (Fig. 3a, Additional file 3: Supplementary Excel File 2). The results were summarized across all ages in four datasets: c_{corr} —Aβ-correlating proteins in cortex; c_{acorr} —Aβ-anticorrelating proteins in cortex; h_{corr} —Aβ-correlating proteins in hippocampus; h_{acorr} —Aβ-anticorrelating proteins in hippocampus (Fig. 3b, Additional file 3: Supplementary Excel File 2). The differential expression of the correlating and anticorrelating proteins (c_{corr} , c_{acorr} , h_{corr} , h_{acorr}) is presented in volcano plots (Fig. 3b, Additional file 3: Supplementary Excel File 2) that were generated with the ggplot2 package in R v.4.2.0. The volcano plots show the protein expression logarithmic fold-changes (\log_{10} FC; x -axis) and the adjusted p -values

($-\log_{10}$ p -value; y -axis). Pearson correlation coefficients between the volumes of accumulated protein Arl8b and 6E10-stained amyloid-beta plaques in hippocampus of 2- (H2), 5- (H5), and 8- (H8) month-old 5xFAD mice were computed with GraphPad Prism v7 (Fig. 5f). Temporal Pearson correlations between A β 42 peptide levels determined by ELISA and A β aggregates detected by MFA in hippocampus (Fig. 1c) and cortex (Additional file 2: Fig. S2b) were calculated in GraphPad Prism v7. To analyze the association of CSF biomarkers [A β (1–42), A β (1–40), A β 42/ A β 40, t-tau, and p-tau] and CSF Arl8b concentrations, a Spearman correlation using GraphPad Prism v7 was performed (Additional file 1: Table S3). For the correlation analysis, Arl8b and biomarker values determined in CSF samples derived from AD patients and control individuals were used. The statistical significance of the association was measured with a two-tailed t -test.

Generation of correlation matrices of differentially expressed proteins

In order to compute the Spearman correlation between DEPs of selected single condition datasets (A2TC, A8TC, A2TH, A5TH and A8TH) in 5xFAD mice (Additional file 3: Supplementary Excel File 1c), a correlation matrix was generated (Fig. 2g) using the packages correlation and corrplot in R v.4.2.0. Since no proteins are significantly changed in the cortex at 5 months (A5TC), this data set is omitted in the correlation analysis. To illustrate an example of strongly associated datasets from Fig. 2g, the correlation between the datasets A2TC and A8TC is shown as a scatterplot (Fig. 2h) representing the expression logarithmic fold-changes (\log_2 FC) of the DEPs in both datasets. The scatterplot was generated using the ggplot2 package in R v.4.2.0. In Fig. 4b, Additional file 2: Fig. S10a and S11, correlation analyses of the DEPs from cortical tissues of 8-month-old mice (DE.cortex.Age8) and DEPs from hippocampal tissues of 5- (DE.hippo.Age5) and 8-month-old mice (DE.hippo.Age8)

with human AD patient data from Johnson 2020 [41] (Additional file 3: Supplementary Excel File 5a), Johnson 2022 [42] (Additional file 3: Supplementary Excel File 5b), and Drummond 2022 [43] (Additional file 3: Supplementary Excel File 5d) and asymptomatic AD patients data (AsymAD) from Johnson 2022 [42] (Additional file 3: Supplementary Excel File 5c) were performed. Strong correlations were selected from Fig. 4b and Additional file 2: Fig. S10a in order to represent them qualitatively in Fig. 4c and Additional file 2: Fig. S10b and to illustrate the concordance using the ggplot2 package in R v.4.2.0. The proteins that are concordantly up- or downregulated in 5xFAD mice and human AD patient brains are shown.

Furthermore, we conducted cross-comparisons of protein abundance data between mouse and human datasets, which are present in all datasets (Additional file 2: Fig. S11) and include all the proteins that were measured (both significant and non-significant, referred to as “all”; Additional file 2: Fig. S11a and b) or those that show significant changes (referred to as “sig”; Additional file 2: Fig. S11c and d).

Generation of protein signatures

The strategy to generate signatures for proteins that are concordantly dysregulated in 5xFAD mice and human AD patient brains is shown schematically in Additional file 2: Fig. S9. Heatmaps were created with GraphPad Prism v7 showing the 15 most down (Sig-, left) and upregulated (Sig+, right) proteins (Fig. 4d, Additional file 3: Supplementary Excel File 7). The top dysregulated proteins were selected from the complete set of proteins that are concordantly dysregulated (Additional file 3: Supplementary Excel File 7).

Enrichment analysis of the dysregulated proteins in brains of 5xFAD mice for specific cell types

The proteomics data from Sharma et al. [49] were used to determine protein markers, expressed exclusively

(See figure on next page.)

Fig. 5 The protein Arl8b is upregulated in hippocampal tissues of 5xFAD mice. **a** Time-dependent change of Arl8b protein abundance in hippocampal and cortical tissues of 5xFAD transgenic animals. LFC, \log_2 fold-change. **b** Hippocampal brain homogenates prepared from four 8-month-old 5xFAD (1 to 4) and control (ctrl; 1 to 4) mice were analyzed by SDS-PAGE and immunoblotting using anti-Arl8b. As a control, a tubulin (anti-alpha Tubulin, #T6074) immunoblot was performed. **c** Quantification of Arl8b expression in relation to tubulin using band intensities of immunoblots in **b**. Relative intensity values (mean \pm SD) are shown for AD ($n=4$) and Ctrl ($n=4$) mice. Statistical significance was assessed between AD and Ctrl mice using an unpaired, two-tailed t -test (*, $p=0.0137$). **d** Immunofluorescence analysis of 5xFAD mouse (8 months) brain slices using AlexaFluor594-labelled 6E10 antibody (red); an anti-Arl8b antibody combined with an AlexaFluor647-labelled anti-rabbit IgG (turquoise) was applied to detect Arl8b. The scale bar shown in the 6E10 image also applies to the Arl8b and merge image. The picture on the right shows a magnification (magnif.) of an area indicated in the merged picture. **e** Brain slices of 8-month-old 5xFAD mice were stained with the primary antibodies indicated in the images. For detection with 352 and Lamp1 antibodies, an AlexaFluor594-labelled anti-mouse IgG (red) was used; for Arl8b detection, an AlexaFluor647-labelled anti-rabbit IgG (turquoise) was applied. Antibody 352 specifically recognizes A β 42 fibrillar aggregates [30]. **f** Pearson correlation between the volumes of Arl8b accumulations and 6E10-stained amyloid-beta plaques in hippocampus of 2- (H2), 5- (H5), and 8- (H8) month-old 5xFAD mice. A total of 60 plaques were analyzed in brain slices derived from 5- and 8-month-old 5xFAD mice. For 2-month-old 5xFAD mice, less than 60 plaques were analyzed, since amyloid burden at this age is low. The statistical significance of the association between the volumes of Arl8b accumulations and 6E10-stained amyloid- β plaques was measured with a two-tailed t -test (*, $p=0.024$; ****, $p<0.0001$)

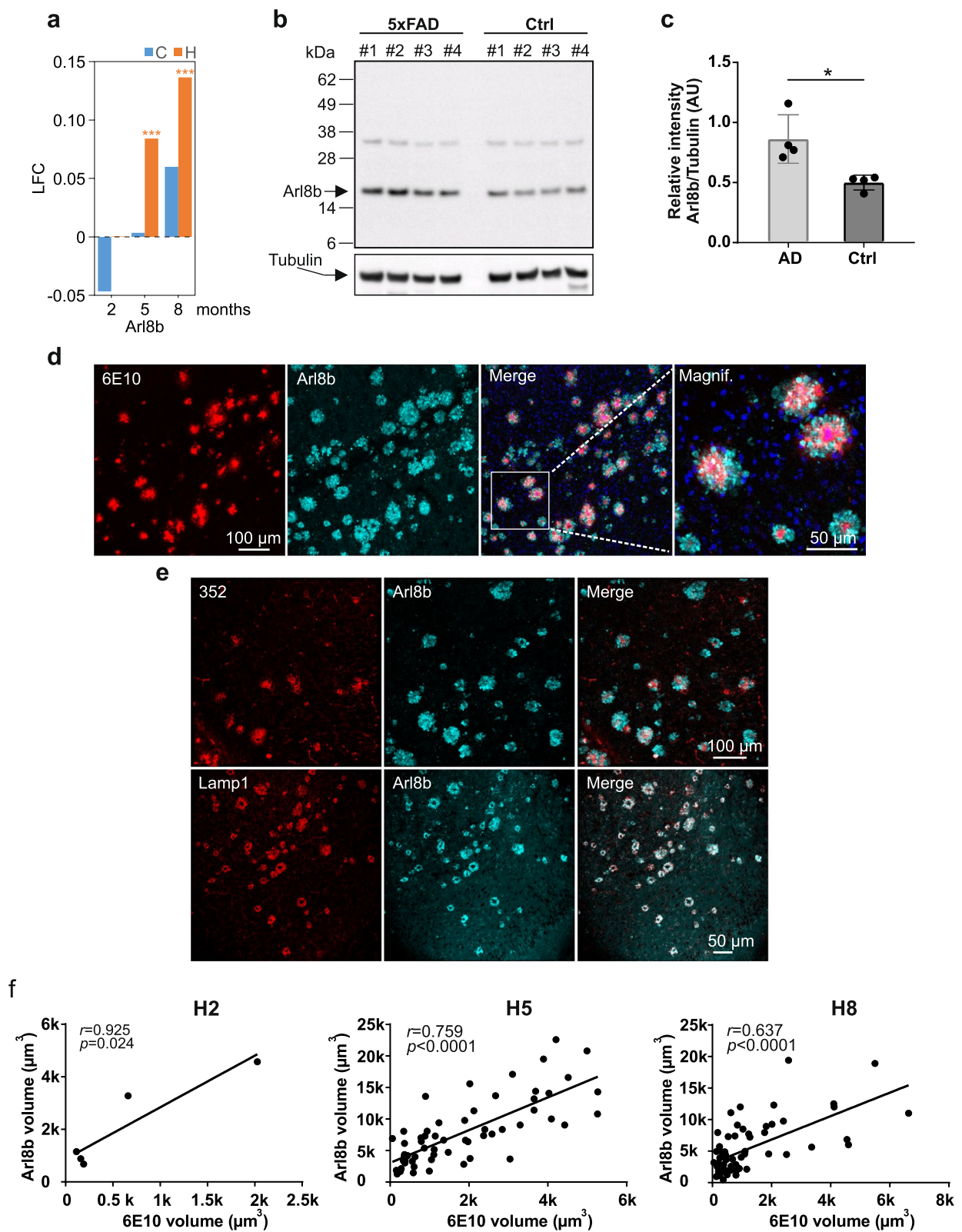


Fig. 5 (See legend on previous page.)

in a subset of brain cells (Additional file 2: Fig. S5). The markers are defined as genes with at least tenfold higher expression in one cell type than in the average of the other cell types. Only the sets of differentially expressed proteins from the pairwise model were analyzed for the enrichment of specific cell types.

Differential centrifugation of mouse brain homogenates and sucrose density gradient centrifugation

The protocol was adopted from a previously reported study [50] with little modifications. Four hippocampi and 4 cortices from 8-month-old 5xFAD mice were homogenized in ice-cold sucrose buffer (320 mM sucrose, 5 mM Hepes pH 7.4) supplemented with protease (Roche #05056489001) and phosphatase inhibitors (Invitrogen #A32957) using the Precellys homogenizer (5800 rpm, 2×15 s with a 30-s break; soft tissue homogenizing kit CK14 – 2 mL, #P000912-LYSKO-A, Bertin Technologies). Each tissue sample (~120 mg cortex) was homogenized in 1.5 ml sucrose buffer. Then the homogenates were pooled. Four hippocampi were pooled (~81 mg) and homogenized in 1.01 ml sucrose buffer. Then, protein homogenates were centrifuged at 1200×g for 20 min at 4 °C. The resulting pellets were discarded and the supernatants collected and centrifuged at 10,000×g for 30 min at 4 °C. The resulting pellets (P10,000×g) were then resuspended in sucrose buffer and 1 ml of each membrane pellet was adjusted to 1.8 M sucrose buffer in 5 mM Hepes (pH 7.4) supplemented with protease and phosphatase inhibitors (giving a final volume of 3 ml) and transferred into Beckman Coulter ultracentrifuge tubes (#355,603). The sucrose gradient was then layered on top of the membrane suspension by 1.33 ml of 1.4 M sucrose buffer with 5 mM Hepes (pH 7.4), 1.33 ml of 1 M sucrose buffer with 5 mM Hepes (pH 7.4), 1.33 ml of 0.6 M sucrose buffer with Hepes (pH 7.4), and 1 ml of 320 mM sucrose buffer with Hepes (pH 7.4). The gradient was centrifuged at 285,000 g at 4 °C for 16 h in a Beckman Optima XPN-90 centrifuge using the 70.1Ti rotor. After centrifugation, the gradient was collected in 0.66 ml fractions from top (fraction 1) to bottom of the tube (fraction 12). The pellet in the tube bottom was resuspended in the last fraction (fraction 12). Equal volumes of each fraction (9.8 µl) were analyzed by immunoblotting.

Ingenuity pathway analysis (IPA)

IPA was performed for several sets of differentially altered proteins.

In Fig. 3g, the 9 identified genes shown in Fig. 3f that are significantly changed both at the transcript and the protein level in 5xFAD brains were examined. In Fig. 4e, IPA was done for proteins which are concomitantly altered in their abundance both in mouse and human brain tissues.

The results of IPA for the differentially expressed proteins across all time points (age 2, 5, and 8) in cortex and hippocampus defined by a “pairwise model” (DE.cortex.Age2, DE.cortex.Age5 and DE.cortex.Age8; DE.hippo.Age2, DE.hippo.Age5 and DE.hippo.Age8) are shown in Additional file 2: Fig. S4a. The results for the DEPs identified through a “full model” (summarized data sets A2TC, A5TC, A8TC and A2TH, A5TH, A8TH) are presented in Additional file 2: Fig. S6a. In Additional file 2: Fig. S7, it was examined whether IPA pathways are significantly enriched among Aβ-correlated and anticorrelated DEPs. Finally, an IPA pathway enrichment analysis of the top 25 Aβ-correlating proteins in the hippocampus was performed, as shown in Additional file 2: Fig. S12b.

IPA is based on a library of canonical pathways [51]. The significance of the association between the examined data set and the canonical pathways was measured with a right-tailed Fisher’s exact test to calculate *p*-values determining the probability that the association between the proteins in the data set and the canonical pathway is explained by chance alone. The *p*-values were adjusted by the Benjamini–Hochberg multiple testing correction. Only the most significant pathways obtained with each subset of DEPs were depicted (Figs. 3g and 4e, Additional file 2: Fig. S4a, S6a and S7).

Analysis of WT expression profiles

To address the question of whether highly expressed mouse brain proteins are more likely to be changed in 5xFAD brains than lowly expressed proteins, we investigated the relationship between WT expression and transgenic effect of the significantly altered proteins (Additional file 3: Supplementary Excel File 1a, b) at month 8 in cortex (DE.Cortex.Age8) and hippocampus (DE.hippo.Age8). First, median splits for the wild-type expression values of the proteins identified at month 8 in cortex and hippocampus were carried out in MS-Excel. Groups of low, medium, and high WT expression were formed, while the proteins in the medium group were omitted for further analysis. We recognized a correlation, i.e., that highly expressed proteins are more likely to be differentially affected than lowly expressed ones by Aβ aggregates in 5xFAD mouse brains (Additional file 2: Fig. S3).

Gene Ontology enrichment analysis

Six time-resolved data sets of DEPs (months 2, 5, and 8, Additional file 3: Supplementary Excel File 1a, b) were selected for a Gene Ontology (GO, RRID:SCR_002811, <http://www.geneontology.org/>) enrichment analysis (Additional file 2: Fig. S4b) that was performed with the Gene Ontology enrichment anaLysis and visualiza-tion tool Gorilla [52]. The shared GO term Molecular

Function in the DEP data sets was measured. The enrichment of Molecular Function terms in the data sets was computed as an exact p -value of a given minimum hypergeometric (mHG) score, corrected for multiple testing determining the probability that the association between the proteins in the data sets and the total number of proteins that map to the GO term is explained by chance alone (Additional file 2: Fig. S4b). The enrichment (Additional file 2: Fig. S4b) is defined as $(b/n)/(B/N)$, where N is the total number of genes; B is the total number of genes associated with a specific GO term; n is the number of genes in the “target set”; and b is the number of genes in the “target set” that are associated with a specific GO term [52].

Another GO enrichment analysis (Additional file 2: Fig. S12c) was performed for the top 25 A β -correlating proteins (Additional file 3: Supplementary Excel File 8b) using the online analysis tool from the PANTHER Classification System (<http://geneontology.org/docs/go-enrichment-analysis/>). The analysis sought to identify cellular components whose enrichment in our data sets was computed as an FDR-corrected p -value. The fold enrichment relative to the entire mouse genome and the number of enriched proteins in our data set per cellular component were also calculated.

Quantification and statistical analysis

Quantification of immunoblots was performed using the iBright Analysis Software (Thermo Fisher Scientific).

The scientific data analysis software GraphPad Prism (GraphPad Software, <https://www.graphpad.com>, RRID:SCR_002798), the R programming environment (R Project for Statistical Computing, RRID:SCR_001905, R Core Development Team, 2006), and MS-Excel were used for data and statistical analysis and graphical representation. Functional analyses of the DEPs were performed using ingenuity pathway analysis [51] and the Gene Ontology enrichment analysis and visualization tool Gorilla [52].

The diagnostic accuracy of Arl8b was evaluated using a receiver operating characteristic (ROC) analysis to calculate the area under the curve (AUC) using datasets of AD patients and controls. The ROC analysis was performed with the GraphPad Prism software applying the linear trapezoid rule for the AUC calculation. The ROC analysis did not include any additional covariates such as age or sex, which are mutually exclusive due to the specific definition of AD patients and controls (see section “Analysis of CSF samples of AD and HD patients”).

Statistical parameters including the value of n (number of independent experimental replications) and the definition of precision measures (arithmetic mean \pm SD)

along with the significance are reported in the figures and figure legends. Data were judged to be statistically significant when $p < 0.05$ (*), $p < 0.01$ (**), $p < 0.001$ (***), and $p < 0.0001$ (****). Specified statistical tests are described in the method details.

Results

Aggregation-prone A β 42 peptides accumulate faster in hippocampus than in cortex of 5xFAD transgenic mice

Previous investigations have demonstrated progressive accumulation of A β 42 peptides in brains of 5xFAD mice [21]. Whether accumulation of A β 42 peptides develops differently in distinct brain regions has not been systematically assessed. Here, we first quantified the abundance of A β 42 peptides in hippocampus and cortex of 2-, 5-, and 8-month-old AD mice and controls using a sandwich ELISA. Brain extracts were supplemented with guanidine HCl to facilitate effective A β 42 peptide detection in protein samples [53]. We observed a time-dependent increase of A β 42 peptides in both hippocampus and cortex of 5xFAD tg mice but not in age-matched control animals (Fig. 1a). However, A β 42 peptide levels were significantly higher in hippocampus than in cortex, indicating that the rate of A β 42 peptide accumulation is distinct in these brain regions. A similar result was also obtained when the abundance of A β 40 peptides was quantified by ELISA (Additional file 2: Fig. S1a). However, it is important to note that in comparison to the measured A β 42 peptide levels A β 40 peptide levels are much lower in 5xFAD brains, confirming previously reported results [21].

To assess whether APP and PS1 expression are distinct in hippocampus and cortex of 5xFAD tg mice, we next quantified transcript levels by qPCR. We measured ~ 1.5 –twofold higher *APP* and *PSEN1* transcript levels in hippocampus than in cortex (Additional file 2: Fig. S1b, c), suggesting that also protein synthesis is higher in hippocampus. This was also confirmed by SDS-PAGE and immunoblotting (Additional file 2: Fig. S1d, e, f). Interestingly, the measured A β 42 peptide levels were \sim threefold higher in hippocampus than in cortex of 8-month-old tg animals (Fig. 1a), suggesting that a ~ 1.5 –twofold higher APP and PS1 protein expression in hippocampus compared to cortex leads to the massive accumulation of A β 42 peptides in this brain region. Interestingly, a much higher amount of proteolytically released ~ 3 kDa A β peptides is present in hippocampus of 8-month-old animals compared to cortex (Additional file 2: Fig. S1d). Together, these results suggest that the process of APP cleavage and A β 42 production is more efficient in hippocampus than in cortex.

Insoluble A β 42 aggregates accumulate in larger amounts in hippocampus than in cortex

To quantify the time-dependent formation of insoluble A β aggregates in brains, we applied a membrane filter assay (MFA), which facilitates the detection of high molecular weight amyloidogenic protein aggregates retained on a cellulose acetate membrane by immunostaining [54]. We found that A β aggregate load in 5xFAD mice was significantly higher in hippocampus than in cortex (Fig. 1b, Additional file 2: Fig. S2a), suggesting that a large fraction of the A β 42 peptides detected by ELISA (Fig. 1a) are aggregated in AD brains. This is supported by statistical analysis indicating that the time-dependent increase in A β 42 peptides in 5xFAD brains and the accumulation of A β aggregates measured by MFA in hippocampus are positively correlated (Fig. 1c). No significant correlation between A β 42 peptide levels and A β aggregate load, however, was obtained for cortical tissue samples (Additional file 2: Fig. S2b). Interestingly, in the hippocampus of 5xFAD tg mice, A β aggregate load increased ~tenfold between 5 and 8 months, while no significant increase was observed in cortex (Fig. 1b).

Next, we performed a systematic immunohistochemical analysis to investigate the abundance of A β amyloid plaques in hippocampus and cortex of 5xFAD tg mice. We applied the A β -reactive monoclonal antibody 6E10 (Additional file 1: Table S1) and first quantified plaque load in AD and control brains. We detected a significantly higher load (measured plaque volume per tissue volume) in hippocampus than in cortex of 5xFAD tg mice (Fig. 1d), essentially confirming the results obtained by MFAs (Fig. 1b). No amyloid plaques were detected with the 6E10 antibody in brains of wild-type control mice (data not shown). A similar result was obtained when the number of amyloid plaques was counted in hippocampus and cortex of 5xFAD tg mice (Fig. 1e). We also quantified the abundance of Thioflavin S (ThioS)-positive amyloid plaques in AD and control mouse brains. ThioS stains the dense core regions in amyloid plaques, which predominantly contain highly stable fibrillar A β 42 structures with a typical cross- β structure [55]. Loosely packed “diffuse” plaques detected by immunohistochemical methods are not stained by ThioS (Fig. 1f). A comparative analysis revealed slightly fewer ThioS-positive A β plaques than 6E10-reactive ones in 5xFAD brains (Fig. 1e). In comparison to cortex, many more ThioS-positive A β plaques were present in the hippocampus (Fig. 1e). Overall, our histological studies revealed that the abundance of A β plaques in hippocampus of 5xFAD tg animals was ~3–fivefold higher than in cortex, indicating that the aggregation rate of A β 42 peptides is different across brain regions.

Finally, we investigated the intracellular accumulation of A β aggregates in 5xFAD brains utilizing an established subcellular fractionation approach [50]. Intracellular membrane fractions were prepared from hippocampal and cortical brain extracts of 8-month-old 5xFAD tg mice by sucrose gradient centrifugation and analyzed by SDS-PAGE and immunoblotting (Additional file 2: Fig. S2c). Established marker proteins such as Calnexin (endoplasmic reticulum), Flotillin (lipid rafts), or Lamp1 (lysosomes) were utilized to assess the association of APP and A β aggregates with different membrane systems. We observed a co-fractionation of high molecular weight, SDS-stable A β aggregates (retained in the stacking gel) with vesicles derived from the ER/endosomal/lysosomal system, indicating that besides extracellular amyloid plaques (Fig. 1e, f) also intracellular A β aggregates accumulate in 5xFAD brains. As expected, the abundance of A β aggregates in hippocampus was higher than in cortex (Fig. 1g, Additional file 2: Fig. S2d, e). Interestingly, we also observed a co-fractionation of A β aggregates with mitochondrial marker proteins (VDAC and NDUFB3), suggesting that also mitochondrial membranes are enriched with our centrifugation procedure. Overall, these biochemical investigations support previously reported immunohistochemical studies, indicating that A β 42 peptides accumulate in cells of 5xFAD brains [21].

Overproduction of mutant variants of APP and PS1 leads to time-dependent proteome changes in hippocampus and cortex of 5xFAD tg mice

To assess whether APP and PS1 overproduction in brains of 5xFAD tg mice is accompanied by global protein expression changes, we performed a quantitative mass spectrometry (MS)-based proteomics analysis. Protein abundance was measured by label-free quantification (LFQ) in hippocampal and cortical tissues prepared from 2-, 5-, and 8-month-old 5xFAD and control mice. By using the quantitative readouts obtained from Max-LFQ analysis [56], we identified ~5000 proteins per tissue on average. We utilized a rather conservative approach to analyze the proteomics data. No imputation was done on missing LFQ intensity values.

First, we compared AD genotypes at indicated ages with their wild-type counterparts (pairwise model). We identified large numbers of differently expressed proteins (DEPs) in both hippocampal and cortical tissues (Fig. 2a, b, Additional file 3: Supplementary Excel File 1a, b). The global proteome response was strongest at 8 months, when deposition of A β aggregates was readily detectable in mouse brains (Fig. 1d), indicating that aggregate formation is associated with perturbation of the mouse brain proteome. In hippocampus, e.g., 57 proteins were differentially expressed at 5 months, while 544 proteins

were changed at 8 months of age (Fig. 2b). Overall, we identified similar numbers of up- and downregulated proteins in hippocampal and cortical tissues (Fig. 2b), although in the cortex at 2 months of age, the number of upregulated proteins was ~sevenfold higher than the number of downregulated ones (Fig. 2b, Additional file 3: Supplementary Excel File 1a, b).

To assess whether A β aggregation predominantly influences the abundance of highly expressed proteins, we utilized the protein abundance measurements in brains of wild-type mice to define groups of proteins with high and low protein expression. Next, we determined whether protein abundance changes detected in 5xFAD brains are more frequent among the highly expressed mouse proteins than among the lowly expressed ones. Interestingly, we found a significantly higher number of A β -associated protein changes among the highly expressed mouse brain proteins (Additional file 2: Fig. S3), supporting our hypothesis that A β aggregation perturbs higher abundant proteins with a higher likelihood than lower abundant proteins.

We performed IPA (ingenuity pathway analysis) for an unbiased assessment of whether observed proteome changes reflect alterations in specific cellular processes and/or pathways. This analysis revealed that many proteins involved in oxidative phosphorylation and mitochondrial functions change in their abundance over time in AD mouse brains (Additional file 2: Fig. S4a), while changes in proteins involved in phagosome maturation and synaptogenesis were predominantly detected relatively late in the disease process (8 months), when large amounts of A β 42 aggregates are already present in AD brains. This was also confirmed by gene ontology (GO) term enrichment analysis (Additional file 2: Fig. S4b).

Finally, we assessed whether the observed protein abundance changes in AD brains originate from different cell types. To address this question, the enrichment of cell type-specific marker proteins, which were previously defined for astrocytes, microglia, neurons, and oligodendrocytes, was investigated [49]. We found only a small number of marker protein changes among the abnormally up- and downregulated proteins in 5xFAD brains (Additional file 2: Fig. S5). However, in hippocampal tissues of 8-month-old animals, multiple neuronal marker proteins were significantly changed, suggesting that the observed global proteome response at least in part originates from A β -perturbed neurons.

The proteome response in cortical and hippocampal tissues of 5xFAD brains is distinct

In order to compare proteome changes between age groups and different tissues, we have limited the differential analysis to proteins reliably measured in each

condition (genotype, age, and tissue) to ensure that the transgene effect difference between conditions can be statistically estimated (for details see “Methods” section). Simple pairwise comparisons would be insufficient because they do not allow the computation of interaction effects. However, this requirement considerably limits the number of proteins that can be modelled: only 2761 (~55% of the originally identified proteins) fulfill the completeness requirements across all conditions.

Utilizing the 2761 proteins in the “full model”, we identified 131 differentially expressed proteins (DEPs) in cortex (2, 5, and 8 months), while 558 DEPs were detected in hippocampal tissues (Fig. 2c, Additional file 3: Supplementary Excel File 1c). Thus, in hippocampal tissues where the time-dependent accumulation of A β aggregates is more rapid than in cortical tissues (Fig. 1a), a ~fourfold higher number of DEPs was observed, suggesting that the proteome response in these brain regions is different.

Next, we focussed on changes in DEPs between time points and tissues. We calculated significant differential protein abundance changes between ages 5 and 2 (A52), 8 and 5 (A85), and 8 and 2 (A82) months for both cortical (C) and hippocampal (H) tissues (T) (Fig. 2c). As expected, in comparison to cortical tissues, the number of significant differential protein abundance changes was ~threefold higher in hippocampal tissues, confirming our initial observations that increased deposition of A β aggregates in brain is associated with higher numbers of DEPs (Fig. 2c). The number of significant differential protein abundance changes was higher between 8 and 2 months (A82TH) than between 5 and 2 (A52TH) or 8 and 5 (A85TH) months, supporting our hypothesis that transgene expression leads to a progressive proteome response that is more pronounced after a time period of 6 (A82) than of 3 (A52 or A85) months. Importantly, differential protein abundance effects were also observed when cortical and hippocampal tissues prepared at 2, 5, and 8 months (A2THC, A5THC, and A8THC) were directly compared with each other (Fig. 2c), substantiating our view that distinct cellular pathways are altered in both tissues upon transgene expression.

In order to identify proteome changes that occur both in cortical and hippocampal tissues, we next looked at overlapping and non-overlapping DEPs in these brain tissues. We found a relatively small fraction of proteins (56 proteins, 8.8%) that were dysregulated upon transgene expression in both hippocampus and cortex (Fig. 2d). A similar result was obtained when proteins, which are significantly increased or decreased in their abundance in hippocampal and cortical tissues, were assessed for overlapping and non-overlapping dysregulated proteins (Fig. 2e, f). Thus, our analysis indicates that most

protein changes observed in hippocampus and cortex are distinct, suggesting that very different cellular pathways and/or processes are altered in these brain regions. This view is also supported by ingenuity pathway analysis (IPA), demonstrating that mostly different cellular pathways are dysregulated over time in these brain regions (Additional file 2: Fig. S6a). We observed dysregulation of mitochondrial processes and mTOR signalling predominantly in cortical tissues, while synaptic processes including long-term potentiation and axon guidance signalling were changed in hippocampal tissues (Additional file 2: Fig. S6a). Pathways altered both in hippocampus and cortex included oxidative phosphorylation, transcription regulation, DNA methylation and repair, indicating that important cellular functions are changed in both tissues. Time-dependent dysregulation of synaptic, lysosomal, and mitochondrial proteins in hippocampal and cortical tissues was confirmed by gene ontology (GO) term enrichment analysis (Additional file 2: Fig. S6b).

To investigate the relationships between protein changes observed in hippocampal and cortical tissues at 2, 5, and 8 months (Additional file 3: Supplementary Excel File 1c), we calculated Spearman correlation coefficients, which can be used to assess the similarity between protein expression data sets. We observed strong correlations, when expression changes of 5- and 8-month-old (A5TH vs. A8TH) hippocampal tissues were compared (Fig. 2g). Similarly, a strong positive correlation was obtained, when expression changes in 8-month-old cortical tissues (A8TC) were compared with expression changes in 5- (A5TH) and 8-month-old (A8TH) hippocampal tissues. This indicates that cortical and hippocampal tissues that contain A β 42 aggregate deposits (Fig. 1d–f) exhibit at least in part a similar protein response. Interestingly, strong anticorrelations were obtained when protein expression changes of 2- and 8-month-old animals were compared (Fig. 2g), indicating that the proteome response in young AD tg mice is the opposite compared to older mice that progressively accumulate A β 42 aggregates. The anticorrelation of protein changes in the cortex of 2- and 8-month-old animals is exemplarily shown in Fig. 2h. Interestingly, in cortical tissues of 2-month-old animals, we observed a strong increase in the abundance of mitochondrial proteins that play a key role in oxidative phosphorylation and ATP production (Fig. 2i), suggesting that expression of mutant human *APP* and *PSEN1* in neurons of young mice is associated with increased mitochondrial activity and ATP production. However, this proteome response gets lost over time when the mice get older concomitantly with the accumulation of A β 42 aggregates, supporting the hypothesis that progressive A β aggregation in neurons impairs critical mitochondrial

functions [57]. Finally, we quantified mRNA changes in cortical and hippocampal tissues and assessed whether the observed time-dependent changes of mitochondrial proteins (Fig. 2i) is also observed at the transcript level (Fig. 2j). Except for one gene, we found no significant transcript changes (Fig. 2j), indicating that the observed mitochondrial protein abundance changes (Fig. 2i) most likely are not caused by transcriptional dysregulation (Fig. 2j).

Overall, these investigations indicate that the proteome response in hippocampus and cortex of *APP* and *PSEN1*-expressing mice is largely distinct. However, in older brains (5 and 8 months), when insoluble A β 42 aggregates are readily detectable, proteome changes in hippocampal and cortical tissues appear to be more similar (Fig. 2g), suggesting that intracellular and/or extracellular A β “aggregate stress” perturbs similar pathways/processes in different brain regions.

Identification of A β -correlated and anticorrelated protein alterations in 5xFAD brains

To explore molecular events associated with progressive A β accumulation, we identified protein abundance changes that are correlated or anticorrelated to the time-dependent accumulation of A β aggregates in hippocampus and cortex of 5xFAD transgenic mice. In total, we identified 699 DEPs (pairwise model, Fig. 2a, b), of which 182 (26.0%) were correlated and 148 (21.2%) were anticorrelated (Additional file 3: Supplementary Excel File 2) to the aggregate load in both brain regions (Fig. 3a, b). As expected, in hippocampal tissue, which contains significantly higher levels of A β aggregates than the cortex (Fig. 1b, d–g), a significantly higher number of correlated and anticorrelated protein changes was found.

Interestingly, we observed a strong positive correlation between the most influential AD risk factor apolipoprotein (ApoE) and the time-dependent accumulation of A β aggregates in both hippocampal and cortical tissues (Fig. 3b), suggesting that this protein gets upregulated in response to A β aggregate deposition. Our pathway analysis (IPA) revealed a significant activation of the LXR/RXR pathway in hippocampal tissues of 5xFAD tg animals (Additional file 2: Fig. S4a). Liver X receptors (LXRs) and retinoid X receptors (RXRs) were reported to function as transcription factors regulating cholesterol and fatty acid homeostasis [58] including the transcriptional activation of the apolipoprotein E (*APOE*) gene [59]. This suggests that the observed activation of the LXR/RXR pathway in 5xFAD brains is accompanied by an upregulation of *APOE* gene expression. To address this question, we quantified mRNAs by RNA-seq and found that *APOE* transcript levels in hippocampal and cortical tissues (5 months) of 5xFAD tg mice are indeed increased

compared to wild-type controls (Fig. 3c). However, in 8-month-old animals, *APOE* transcript levels were decreased in cortical but not in hippocampal tissues, suggesting that at a later stage transcriptional regulation of *APOE* expression is distinct in these tissues. Strikingly, a very pronounced time-dependent increase of ApoE protein levels was detected in both brain regions at 5 and 8 months, indicating that *APOE* transcript and protein levels in cortical tissues of 8-month-old animals are not well correlated (Fig. 3d).

Also, we found that the proteins C1qb, Hexb, and Acat2 are strongly correlated with the appearance of A β aggregates in both brain regions in 5xFAD mice (Fig. 3b). Strikingly, all these proteins have been previously linked to AD as well as to cellular processes that control the progressive accumulation of A β aggregates [17, 60]. C1qb is the initiating protein of the classical complement cascade, which associates with A β pathology in patient brains and was previously shown to mediate synapse loss in transgenic AD models [61]. The gene encoding Hexb was previously identified as a putative AD risk gene. It is important for lysosome function and influences A β accumulation in mouse brains [62]. Acat2 is central to lipid metabolism and inhibitors of this protein were shown to modulate A β production and reduce A β accumulation in a transgenic model of AD [63]. In contrast to these positively correlated proteins, we found Arpc5 and Glrx to be significantly anticorrelated to A β accumulation in both brain regions (Fig. 3b), suggesting that their activity gets decreased upon progressive A β aggregation in 5xFAD brains. Arpc5 is a subunit of the Arp2/3 complex that promotes actin filament assembly [64] and is known to influence neurite outgrowth. A direct link to AD has not been described; however, it is well-known that progressive A β accumulation perturbs actin dynamics in neuronal cells [65]. Glrx, a member of the glutaredoxin family, was previously shown to influence cognitive deficits in an AD mouse model [66].

Finally, we performed IPA to elucidate subcellular pathways that are potentially influenced by progressive A β 42 accumulation in brains of 5xFAD transgenic mice. We observed that multiple proteins involved in synaptogenesis signalling and phagosome maturation are altered significantly in their abundance in hippocampal tissues of 5xFAD (Additional file 2: Fig. S7), suggesting that progressive A β 42 accumulation in this brain region perturbs critical synapse functions. This is in agreement with previous observations indicating that small A β 42 assemblies, often termed oligomers, target synapses and can perturb the activity of specific synaptic proteins [18, 67]. Interestingly, in cortical tissues, where the time-dependent deposition of A β 42 aggregates is significantly lower compared to hippocampal

tissues (Fig. 1b, d–g), we observed no synaptic protein changes (Additional file 2: Fig. S7), supporting our hypothesis that A β 42 aggregation and perturbation of protein homeostasis at synapses are linked. Overall, these investigations indicate that progressive accumulation of A β 42 peptides in AD mouse brains is associated with alterations in synaptic functions, which may lead to neuronal dysfunction and memory impairment.

A β -correlated and anticorrelated proteome and transcriptome changes are largely distinct in 5xFAD brains

We generated mRNA expression data sets by RNA-seq (Additional file 3: Supplementary Excel File 3) to compare proteome and transcriptome changes in hippocampal and cortical tissues of 2-, 5-, and 8-month-old 5xFAD transgenic mice and age-matched wild-type controls. Here, we specifically focused on transcripts that encode proteins whose abundance is significantly changed in 5xFAD brains and that are also correlated or anticorrelated to the A β aggregate load. As expected, we detected transcripts for all of the 329 significantly dysregulated A β -correlated and anticorrelated proteins in 5xFAD brains (Fig. 3e, Additional file 3: Supplementary Excel File 3). However, only a small fraction of these transcripts (2.8%) was significantly changed in 5xFAD brains (Fig. 3e), indicating that most of the protein abundance changes associated with A β aggregation in 5xFAD brains are caused by posttranscriptional mechanisms rather than transcriptional dysregulation. We identified 9 genes that are significantly changed both at the transcript and the protein level in 5xFAD brains (Fig. 3f). Interestingly, a large fraction of these genes encodes proteins that play a functional role in the complement system (C1qa, C1qb, and C1qc), suggesting that transcriptome changes predominantly drive microglia activation and inflammatory processes in 5xFAD brains. This is also supported by IPA, indicating that proteins involved in the complement system are overrepresented among the transcriptionally dysregulated proteins (Fig. 3g, Additional file 3: Supplementary Excel File 4). However, it is important to note that also the abundance of proteins with specific functions in lysosomes (Hexb), metabolic processes (Acat2), and protein degradation pathways (Ctsd, Cst3) are transcriptionally regulated in 5xFAD brains.

A fraction of dysregulated proteins in 5xFAD brains is concordantly altered in postmortem brains of AD patients

Next, we assessed whether proteins that change in their abundance in brains of 5xFAD mice (Fig. 2) overlap with proteome changes detected in postmortem brains of AD patients. For our comparisons, we focussed on

two recently reported large-scale proteomics studies (J20 and J22) that measured the abundances of human proteins in postmortem brains of AD patients and controls using different quantitative mass spectrometry approaches [41, 42]. In total, in J20 and J22, 3950 significantly altered AD-associated human proteins were identified. In addition, we compared our DEPs from mouse brains with a recently reported amyloid plaque proteome (termed D22; 816 proteins), which was obtained by label-free MS analysis of microdissected A β plaques [43]. Here, we focused our efforts on protein abundance changes detected in 8-month-old hippocampal and cortical mouse tissues, which contain high levels of potentially proteotoxic A β 42 aggregates (Fig. 1d, e). In addition, protein abundance changes in 5-month-old hippocampal tissues, which also contain significant amounts of amyloidogenic protein aggregates, were compared with patient protein measurements. We found a substantial overlap between mouse (Additional file 3: Supplementary Excel File 1a) and human DEPs (Fig. 4a, Additional file 2: Fig. S8 and Additional file 3: Supplementary Excel Files 5a-d and 6), indicating that 5xFAD tg mice at least in part recapitulate the proteomic changes observed in AD patient brains. In total, from the 3718 significantly changed proteins in mouse (H5, H8, and C8) and human brains (D22, J20, and J22), 447 (12%) proteins were overlapping. Interestingly, a small number of proteins such as ApoE, Clu, or NDUFA12 were significantly altered in all investigated data sets, suggesting that these amyloid-associated proteins robustly reflect the amyloid state both in patient and mouse brains.

To assess whether the observed protein changes in mouse and patient brains are similar, we calculated Spearman correlation coefficients for all pairwise data cross-comparisons (Fig. 4b, c). Strikingly, we observed a strong correlation between the protein measurements in hippocampal or cortical tissues of 5xFAD mice and the protein measurements in patient amyloid plaques (D22 data set), indicating that in 5xFAD brains multiple potentially disease-relevant protein changes are recapitulated that are also detectable in amyloid plaques of patient brains [43]. Also, moderate positive correlations were obtained when protein measurements of cortical (8 months) or hippocampal (5 months) tissues were compared with the large-scale proteomics data sets J20 or J22. This supports our hypothesis that disease-relevant amyloid-related proteome changes are recapitulated in 5xFAD mice. Interestingly, our analysis indicates that protein changes that are measured in mouse brain tissues with a relatively low amount of A β aggregates (e.g., 5-month-old hippocampal tissues or 8-month-old cortical tissues)

were better correlated to AD patient protein changes (J20 and J22 data sets) than protein changes measured in 8-month-old hippocampal tissues (Fig. 4b), which contain a very high amount of insoluble A β aggregates (Fig. 1b). This indicates that young 5xFAD transgenic mice with low amounts of A β aggregates in their brains mimic the disease state in patient brains better than older mice with very high amounts of aggregates. As expected, strong positive correlations were obtained when protein measurements of different human brain samples were compared in a pairwise manner (e.g., D22 with J22; Fig. 4b).

Next, utilizing the results from all data cross-comparisons, we generated a data set that exclusively contains proteins, which are concomitantly altered in their abundance both in mouse and human brain tissues. In total, 140 potential AD-relevant protein changes were defined (Additional file 3: Supplementary Excel File 7), of which 67 (47.9%) were abnormally up- and 73 (52.1%) were downregulated in hippocampal and/or cortical mouse tissues of 5xFAD brains. The top 15 proteins with the highest fold-changes from this data set were selected in order to define potentially patient-relevant mouse protein signatures (Sig+ and Sig-; Additional file 2: Fig. S9, Additional file 3: Supplementary Excel File 7). As shown in Fig. 4d, proteins such as ApoE, Clu, and GFAP are strongly upregulated both in 5xFAD and AD patient brains, while proteins such as CNP, NDUFA12, and MBP are downregulated. We also performed IPA using the data set of concordantly changed mouse proteins (Additional file 3: Supplementary Excel File 7). Strikingly, proteins that play a key role in mitochondria and synapses were enriched in this data set (Fig. 4e, Additional file 3: Supplementary Excel File 4), supporting our hypothesis that “A β aggregate stress” perturbs important mitochondrial and synaptic functions both in mouse and human AD brains.

For independent validation, a comprehensive proteomics data set obtained from brains of asymptomatic AD patients (AsymAD) was utilized for comparison with mouse proteomics data sets. AsymAD cases have a neuropathological burden of A β plaques and tau neurofibrillary tangles similar to AD cases but without cognitive impairment near time of death, which is consistent with an early preclinical stage of AD [68]. We again performed data cross-comparisons with significant protein abundance changes detected in hippocampal (H5 and H8) and cortical (C8) tissues that contain significant amounts of A β aggregates (Fig. 1d). Similar to comparisons with proteomics data from AD patients (Fig. 4a, b, Additional file 2: Fig. S8 and Additional file 3: Supplementary Excel File 6), we obtained a substantial overlap between AsymAD and mouse DEPs

(Additional file 2: Fig. S10a, Additional file 3: Supplementary Excel File 6). Also, correlations between AsymAD and mouse data were similar to correlations obtained with AD patient data (Additional file 2: Fig. S10a, b), confirming that potentially disease-relevant protein changes are robustly recapitulated in 5xFAD brains with low amounts of A β aggregates. This is also observed when concordantly altered protein changes are considered (Additional file 2: Fig. S10b, c), confirming that protein changes detected in patient and AsymAD brains are also observed in 5xFAD mouse brain tissues. Overall, these investigations indicate that proteome changes detected in brains of AD and AsymAD patients are robustly recapitulated in brains of transgenic 5xFAD mice that contain amyloidogenic A β aggregates.

Finally, we performed data cross-comparisons utilizing data sets (mouse and human) that contain all measured proteins (significant and non-significant; “all”) or just significantly changed proteins “sig”. Hippocampal (H5+H8) and cortical (C8) mouse data sets obtained from tissues that contain insoluble A β aggregates were exclusively used for these comparisons (see Fig. 1a–f). In addition, we combined the previously reported proteomics data sets from the studies J20, J22, and J22_Asym [40, 41] and generated two comprehensive human cortical data sets termed “all_human” and “sig_human” for data cross-comparisons. Our data comparisons revealed a substantial overlap between mouse and human DEPs (Additional file 2: Fig. S11a–d). Then, we calculated Spearman correlation coefficients for four data cross-comparisons (all_mouse DE.cortex.Age8 vs. all_human; all_mouse DE.hippo.Age5+DE.hippo.Age8 vs. all_human; sig_mouse DE.cortex.Age8 vs. sig_human and sig_mouse DE.hippo.Age5+DE.hippo.Age8 vs. sig_human). We found highly significant moderate correlations when cortical mouse and human data sets were compared (Additional file 2: Fig. S11a, c), confirming our hypothesis that the mouse model data properly recapitulate the previously reported human brain data. In comparison, no or very weak correlations were obtained when mouse hippocampal data were compared with human cortical data. This is expected because protein expression in hippocampal tissues is distinct from cortical tissues [49]. Thus, our additional data cross-comparisons strongly support our working hypothesis that DEPs detected in 5xFAD brains at least in part are predictive for the disease situation in AD patient brains.

The levels of the Arf-like GTPase Arl8b are abnormally increased in hippocampal tissues of 5xFAD mice

In its earliest clinical phase, AD is characterized by memory impairment [69] and changes of the lysosomal network,

which consists of an interconnected vesicular network of endosomes, lysosomes, and autophagosomes and plays a critical role in A β clearance in neurons [70, 71]. Therefore, we next searched for neuronal proteins in the mouse proteomics data set that are (1) concordantly dysregulated in mouse and human data sets, (2) among the top 25 A β -correlated proteins in mouse hippocampal tissues, and (3) are previously well-described lysosomal network proteins. Using a step-by-step data filtering approach (s. Additional file 2: Fig. S12a and Additional file 3: Supplementary Excel File 8a), we identified the top 25 A β -correlated proteins (Additional file 3: Supplementary Excel File 8b) that are also concordantly altered in human brains. Among these proteins, many proteins are associated with lysosomes or play a functional role in protein degradation pathways such as autophagy (Additional file 2: Fig. S12b, c). Finally, among the lysosome-associated proteins, two proteins (Arl8b [72, 73] and Lamp1 [74]) that meet our criteria and potentially play a critical role in AD brains were selected. Because the ARF-like GTPase Arl8b in comparison to Lamp1 [75, 76] previously was only studied marginally in the context of AD, we decided to focus on this protein for further validation experiments and potential biomarker studies in CSF.

To independently validate the changes in Arl8b abundance initially observed with mass spectrometry (Fig. 5a), we analyzed protein extracts prepared from hippocampal tissues of 8-month-old 5xFAD and control mice by SDS-PAGE and immunoblotting. We confirmed that protein levels of Arl8b in AD mouse brains are significantly increased compared to age-matched controls (Fig. 5b, c).

Next, we assessed the abundance of Arl8b in 5xFAD brains by immunohistochemistry. Strikingly, we observed a time-dependent accumulation of Arl8b in ring-like structures surrounding A β 42 amyloid plaques (Fig. 5d and Additional file 2: Fig. S13). These structures have been reported to be axonal lysosome accumulations formed in close vicinity to amyloid plaques in AD brains [77]. To determine whether the observed Arl8b-positive structures are indeed lysosomal accumulations, we stained brain slices with an antibody that recognizes the lysosomal marker protein Lamp1 ([74], Additional file 1: Table S1). As expected, we observed co-staining of Arl8b and Lamp1 in 5xFAD brains (Fig. 5e). The formation of A β aggregates in mouse brains was confirmed with the monoclonal antibody 352 (Fig. 5e, Additional file 1: Table S1), which specifically recognizes A β 42 fibrillar aggregates but not soluble monomers *in vitro* [30].

Finally, we assessed the relationship between the volume of A β 42 plaques in 2-, 5-, and 8-month-old 5xFAD mice and the volume of Arl8b-positive lysosomal structures accumulating in their vicinity. We found a strong correlation between Arl8b- and 6E10-stained structures in hippocampal tissues of all three ages (Fig. 5f),

suggesting that the time-dependent formation of amyloid plaques determines the size of the adjacent Arl8b-positive lysosomal structures in 5xFAD brains. An association of Arl8b with lysosomal membranes and proteins has previously been described [72, 73], supporting our immunobiological results.

Arl8b protein levels are abnormally increased in postmortem brain tissues and CSF samples of AD patients

To analyze whether Arl8b accumulates in AD patient brains, we investigated protein extracts prepared from postmortem brain tissues of AD patients and age-matched controls (10 each) using a membrane filter assay (MFA) [54]. With this method, large protein aggregates, e.g., A β and tau assemblies, retained on a cellulose acetate membrane after filtration (pore size 0.2 μ m), can be detected by immunoblotting [30, 38]. We found that the immunoreactivity of Arl8a and Arl8b, both specifically recognized by the anti-Arl8a/b antibody (Additional file 1: Table S1), is significantly increased in AD patient brains compared to age-matched controls (Fig. 6a, b), indicating that the abundance of these functionally and structurally closely related proteins is abnormally elevated in AD patient brains. A similar result was obtained with an Arl8b-specific antibody (Additional file 2: Fig. S14a, b).

Finally, we investigated the levels of Arl8b in cerebrospinal fluid (CSF) of AD patients and control individuals using an ELISA. The demographic, clinical, and CSF biomarker characteristics of AD patients and control individuals are summarized in Additional file 1: Table S2. Strikingly, we measured significantly higher Arl8b protein levels in CSF samples of AD patients compared to controls (Fig. 6c), confirming that protein abundance is abnormally increased in AD brains. In strong contrast, no significant increase of Arl8b protein levels was measured when CSF samples obtained from HD patients and controls were analyzed with ELISA (Fig. 6d), indicating that the observed increase in protein abundance is an AD-specific phenomenon. We next assessed the correlations of Arl8b protein levels with other well-established AD biomarkers such as A β (1–42), A β (1–40), A β 42/ A β 40, t-tau, and p-tau [68]. Spearman correlation analysis revealed a significant moderate negative correlation between Arl8b protein levels and CSF A β 42/ A β 40 ratios ($r_s = -0.405$; $p = 0.0002$), supporting our hypothesis that increased Arl8b protein levels are associated with the deposition of A β 42 protein aggregates in patient brains (Additional file 1: Table S3). A weak negative correlation was also observed with A β (1–42) CSF peptide levels, while no significant correlation was obtained with A β

(1–40) levels. Interestingly, we also observed a moderate positive correlation between Arl8b and p-tau protein levels in CSF samples, suggesting that an increase of Arl8b is also associated with cognitive impairment in AD patients. This is also supported by total tau (t-tau) measurements, which show a weak correlation to Arl8b protein levels. Finally, we performed a ROC analysis and calculated an area under the curve (AUC) of 0.73 (Fig. 6e), confirming that Arl8b measurements can be utilized to differentiate between AD patients and controls. Overall, these studies suggest that Arl8b together with other biomarkers might have potential as a novel CSF biomarker for patient stratification, facilitating the measurement of abnormal lysosome structures, which form early in neurons and progressively accumulate in AD patient brains.

Discussion

The progressive deposition of A β 42 peptides in amyloid plaques and intraneuronal structures in patient brains is a pathological hallmark of AD [78]. A β aggregates in patient brains are detected before the onset of neurodegeneration and memory impairment in AD patients [79], indicating that their formation is an early event in pathogenesis. However, it was shown reproducibly that the formation of A β plaques in patient brains is not a good predictor of neurodegeneration [80]. This suggests that A β aggregation is relevant but not solely responsible for disease onset and that other molecular changes drive progressive neurodegeneration in patient brain. Evidence was reported that A β aggregation in disease models triggers tau accumulation, which is a good predictor of neurodegeneration and memory impairment [81, 82]. Thus, accumulation of A β peptides in patient brains is broadly regarded as a key early event in pathogenesis, leading to downstream neuropathological changes such as the accumulation of tau or abnormal microglia activation and eventually to neurodegeneration.

Here, we report protein abundance changes associated with the progressive accumulation of A β 42 aggregates in brains of 5xFAD tg mice (Figs. 2a–i and 3a–f). 5xFAD tg mice are a well-characterized disease model expressing two human genes (*APP* and *PSEN1*) with familial AD mutations in neurons, leading to the rapid accumulation of intra- and extracellular A β 42 aggregates in brains [21]. Progressive deposition of A β 42 structures is accompanied by microglia activation, a change of synaptic proteins and neurodegeneration, suggesting that A β 42 aggregation in 5xFAD mouse brains drives important downstream proteomic changes that are also observed in AD patient brains. Various proteomics and transcriptomics studies have uncovered that microglial phagocytosis

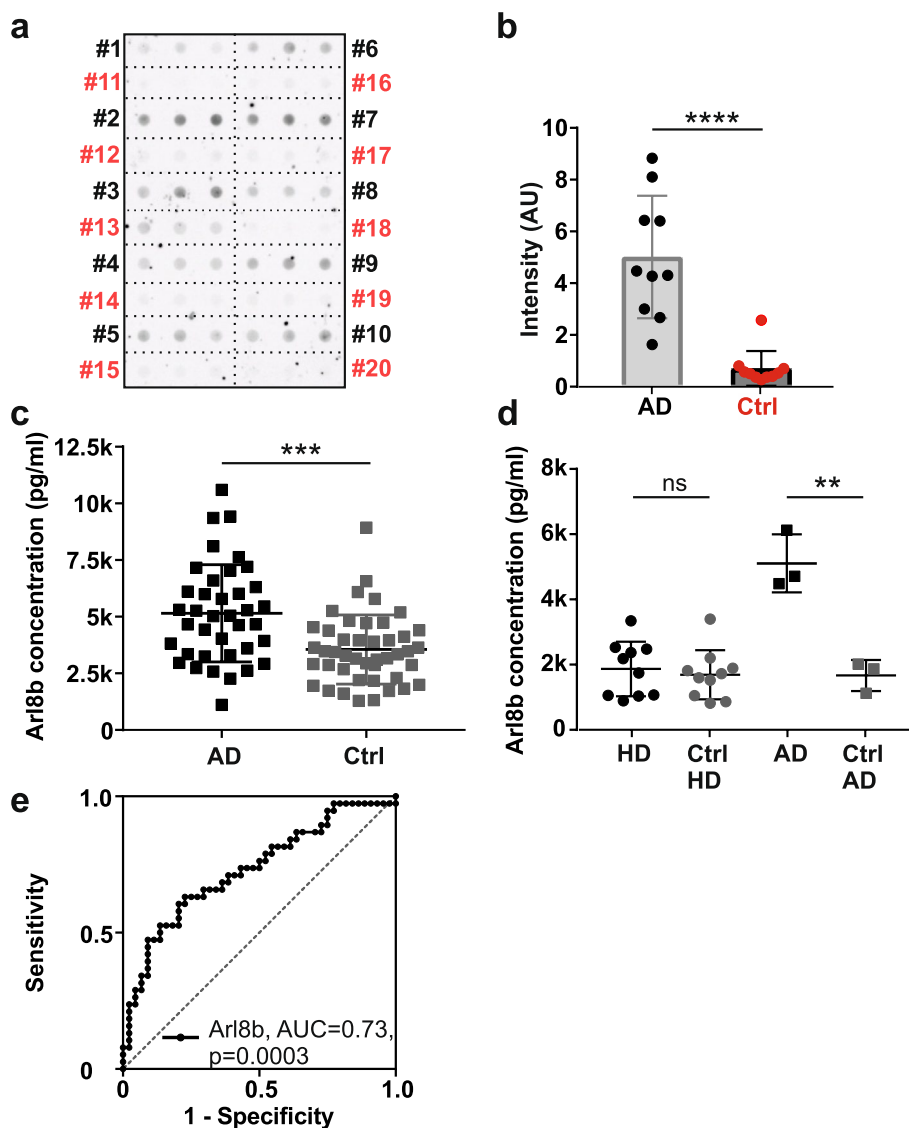


Fig. 6 Analysis of Arl8b expression in human brain and CSF samples. **a** Detection of Arl8b protein aggregates in postmortem brain homogenates of 10 AD patients (1 to 10, black lettering) and 10 age-matched controls (11 to 20, red lettering) using a native MFA. Triplicates per sample were filtered. For immunoblotting, an anti-Arl8a/b antibody was used. **b** Quantification of protein aggregates retained on filter membrane in **a** was performed using Aida image analysis software. Data are expressed as mean \pm SD. The statistical significance was assessed with an unpaired, two-tailed *t*-test (****, $p < 0.0001$). **c** Determination of Arl8b concentrations in CSF samples of 38 AD patients and 44 control individuals (Ctrl) using an ELISA. Data represent mean \pm SD. Statistical significance was determined using an unpaired, two-tailed *t*-test (***, $p = 0.0002$). **d** Arl8b ELISA using CSF samples of 10 Huntington's disease (HD) patients, 10 controls (Ctrl HD), 3 AD patients, and 3 controls (Ctrl AD). Data are mean \pm SD. Statistical significance was evaluated using an unpaired, two-tailed *t*-test between HD and Ctrl HD, and AD and Ctrl AD groups (**, $p = 0.0041$). **e** ROC analysis of Arl8b levels derived from both AD patients and control individuals using GraphPad Prism software. The area under the curve (AUC) is 0.73 with a *p*-value of 0.0003

is significantly perturbed in 5xFAD brains, suggesting that extracellular A β 42 aggregation predominantly leads to an inflammatory response that over time is associated with neuronal dysfunction and toxicity [83]. However, it is unclear whether proteome changes that accompany the accumulation of intra- and extracellular A β 42 aggregates in 5xFAD are conserved in patient brains.

Based on our comparative analyses (Fig. 4a–d), we suggest that progressive A β aggregation in 5xFAD and AD patient brains may lead to similar perturbations of the proteome and could provide valuable information about critical pathways perturbed in disease. We hypothesize that the proteome response to A β aggregate stress is conserved in mouse and human brains to a considerable

extent and at least a fraction of the proteome changes observed in patient brains may be caused by progressive A β aggregation. Interestingly, our proteome-based data cross-comparisons indicate that protein changes in mouse brain tissues with a relatively low amount of A β aggregates are more similar to protein changes in AD patient brains than protein changes in tissues, which contain a high A β aggregate load (Fig. 4b). This suggests that overexpression of mutant variants of *APP* and *PSEN1* in hippocampal neurons of 5xFAD mice after some time (8 months) leads to a proteome response that is distinct from the situation in patient brains. Together, these studies indicate that 5xFAD transgenic animals recapitulate important features of the pathogenic process in patient brains. However, timing and brain region-specific investigations are critical for the detection of potential disease-relevant proteome changes in mouse brains. We propose that the proteome changes measured in the hippocampus of 5-month-old 5xFAD mice recapitulate the disease situation in AD patient brains better than the protein changes measured in 8-month-old animals, where massive amounts of A β 42 aggregates are detectable by immunohistochemistry or biochemical methods. In comparison, the situation is different when proteome changes in cortical tissues of 5xFAD mice are assessed where the rate of A β 42 aggregate accumulation is significantly slower than in hippocampal tissues (Fig. 1d). Thus, our investigations suggest that 5xFAD mice with their massive accumulation of A β 42 aggregates in a relatively short time (2–8 months) are a useful model to study the impact of A β aggregation on the proteome. We propose that pharmacological interventions in 5xFAD mice may have a predictive value for AD patients if conserved A β 42 aggregate-associated proteome changes could be reversed by drug treatment. Previously, small molecules and therapeutic antibodies that directly target A β aggregate assemblies and reduce their propagation in model systems have been described [30, 84]. Whether their application might reverse the proteome changes in 5xFAD brains defined here would need to be assessed.

We provide evidence that progressive A β 42 aggregation is associated with a reduced abundance of multiple mitochondrial proteins (Fig. 2i), suggesting that A β 42 accumulation drives mitochondrial dysfunction in 5xFAD brains. Strikingly, a loss of mitochondrial proteins is also a characteristic feature of AD brains [85], supporting the hypothesis that decreased energy production is associated with cognitive decline in AD patients [86]. This view is supported by a recent large-scale proteome study, indicating that a stable cognitive trajectory in advanced age is associated with higher levels of mitochondrial proteins and increased neuronal

mitochondrial activity [87]. Enhancing mitochondrial proteostasis with pharmaceutical compounds reduced A β aggregate-induced proteotoxicity in model systems [19], substantiating the link between A β pathology and mitochondrial dysfunction. The underlying molecular mechanism by which the A β 42 peptides in 5xFAD brains perturb the mitochondrial proteome currently remains unclear, however. We found here that both APP and insoluble A β 42 aggregates indeed co-fractionate with mitochondrial membranes in 5xFAD brains, suggesting that they also might interact with mitochondria (Fig. 1g). It was previously reported that APP and its cleavage products accumulate in mitochondria [88, 89], suggesting they might directly perturb the electron transport machinery, thereby decreasing ATP synthesis [90]. However, toxicity might also be caused by A β 42 assemblies acting on regulators of gene transcription such as H2AFZ (Fig. 3b) or on the surface of mitochondria, perturbing the import of critical mitochondrial proteins or influencing fission, transport, or degradation of mitochondria [86]. Further mechanistic investigations are clearly necessary to elucidate the link between A β 42 aggregation and mitochondrial dysfunction in 5xFAD brains and other model systems. Besides oxidative phosphorylation in mitochondria, various pathways and subcellular processes such as carbohydrate metabolism or synaptogenesis are potentially perturbed in response to A β 42 accumulation in 5xFAD brains (Fig. 4e and Additional file 2: Fig. S7). The impact of A β 42 overproduction on brain physiology is likely highly complex and brain region specific. Links between energy metabolism, synaptic transmission, and inflammation have been described in the aging brain and in AD [91, 92], suggesting that the generation of multiscale causal networks and the integration of additional information such as protein–protein interaction data is necessary to elucidate the specific role of A β aggregates in mouse brains.

Our studies indicate that progressive A β 42 aggregation leads to the time-dependent accumulation of the small GTPase Arl8b in brains of 5xFAD mice (Fig. 5a–f). This protein mediates axonal transport of both lysosomes and synaptic vesicles in neurons [93, 94], suggesting that its function is of critical importance for the maintenance of synaptic compartments and neurotransmission. This is supported by gene knock-down experiments in hippocampal neurons indicating that loss of Arl8b leads to the accumulation of synaptic vesicles (SVs) in neuronal cell bodies and the depletion of active zone proteins from presynaptic sites [95]. Our studies showed that Arl8b as well as lysosomal proteins such as LAMP1 are enriched in the vicinity of extracellular amyloid plaques, indicating that progressive A β 42 aggregation is critical for the accumulation of lysosomal structures in 5xFAD brains

(Fig. 5d–f). This is in agreement with previous investigations demonstrating that protease-deficient axonal lysosomes accumulate in the vicinity of amyloid plaques [77]. Recently, an accumulation of the GTPase Arl8b in the vicinity of amyloid plaques in patient brains has also been demonstrated by immunohistochemistry [43]. Its specific role in AD, however, is currently unclear. Recent investigations in *Caenorhabditis elegans* indicate that overexpression of Arl8b significantly decreases A β aggregation and neurotoxicity [96], suggesting that the accumulation of lysosomal membranes with Arl8b in AD mouse brains may be a protective cellular response that promotes the degeneration of A β aggregates. This view is also supported by a recent study indicating that elevated Arl8b expression rescues lysosome transport and thereby reduces axonal autophagic stress and neuron death in Niemann-Pick disease [97]. Thus, increased levels of Arl8b in AD patient brains may be an indication of increased lysosomal activity to protect neurons from A β aggregate stress. However, Arl8b accumulation may also stimulate lysosome exocytosis that is known to affect APP processing and A β secretion [98]. An increase of lysosomal exocytosis has been described in cancer cells overproducing Arl8b, hinting that this process may also be enhanced in neuronal cells, which contain lysosome-like organelles with high local concentrations of Arl8b (Fig. 5d). However, the functional consequences of Arl8b accumulation in axonal lysosomes in the presence of amyloid aggregates need to be studied further in model systems.

Interestingly, our investigations indicate that Arl8b protein levels are significantly increased both in CSF and postmortem brain tissues of AD patients (Fig. 6a–d), suggesting that this protein may have the potential to be utilized as a biomarker to monitor lysosomal function or dysfunction in AD brains. Lysosomal network proteins such as Lamp1 or Lamp2 have been shown previously to have potential as CSF biomarkers for AD [76]. Also, cell-based experiments have shown that lysosomal cathepsins play an important role in the generation of A β peptides [99]. Lysosomal membrane alterations have been observed in brains of AD patients [100], and accumulation of A β 42 in neuronal cells was shown to lead to changes in the abundance of lysosomal organelles and cell death [101]. Thus, it seems adequate to speculate that lysosome-associated proteins that change in their abundance in AD brains are putative biomarkers that might predict disease development or progression. Currently, the well-established pathological polypeptides such as total tau, phospho-tau, and A β 42 are measured in CSF to detect incipient and established AD in patients [68, 102]. However, major research efforts are on the way to finding additional fluid biomarkers to predict disease onset and

monitor progression more accurately [41, 42, 85, 102–104]. Previous studies have shown, e.g., that neurofilament light chain (NFL) and neurogranin are promising AD biomarkers [105, 106]. We envision that a better definition of AD will clearly require a more accurate characterization and understanding of the sequence of events that lead to cognitive impairment. The measurement of Arl8b protein levels in CSF or plasma of AD patients might help to meet this goal. However, more comprehensive future studies with symptomatic and asymptomatic AD patients and controls will be necessary to further assess the predictive power of Arl8b as a clinical biomarker.

Conclusions

Our studies indicate that A β 42-driven aggregate formation is associated with time-dependent and brain region-specific proteome changes in 5xFAD mouse brains. We detected 329 dysregulated proteins correlating or anticorrelating with A β aggregation in hippocampus and cortex of 5xFAD mice. Most of these protein changes were caused by posttranscriptional mechanisms, only a minor part was associated with transcriptional dysregulation. A fraction of the A β -correlated and anticorrelated DEPs was conserved in postmortem brains of AD patients revealing that proteome changes in 5xFAD mice recapitulate disease-relevant changes in AD patient brains. Among the group of conserved and strongly A β 42-correlating proteins, we have found the lysosome-associated protein Arl8b, which is present in increased levels in CSF samples of AD patients and might have potential as an AD biomarker.

Abbreviations

FAD	Familial Alzheimer's disease
A β	Amyloid- β
AD	Alzheimer's disease
MS	Mass spectrometry
LFQ	Label-free quantification
vs.	Versus
CSF	Cerebrospinal fluid
NFTs	Neurofibrillary tangles
wt	Wild-type
tg	Transgenic
IB	Immunoblotting
IS	Immunostaining
MFA	Membrane filter assay
HD	Huntington's disease
PCR	Polymerase chain reaction
FDR	False discovery rate
DEP	Differentially expressed protein
DEG	Differentially expressed gene
OXPPOS	Oxidative phosphorylation
IPA	Ingenuity pathway analysis
GO	Gene ontology
Q	Quadrant
r	Pearson correlation coefficient
SV	Synaptic vesicle
NFL	Neurofilament light chain

ctrl	Control
SD	Standard deviation
M	Month
H, h	Hippocampus
C, c	Cortex
AU	Arbitrary unit
corr	Correlated
acorr	Anticorrelated
FC	Fold-change
Agg	Aggregate

Supplementary Information

The online version contains supplementary material available at <https://doi.org/10.1186/s13073-023-01206-2>.

Additional file 1: Table S1. Commercial antibodies used in this study. **Table S2.** Characteristics of AD and HD patients and corresponding controls. **Table S3.** Spearman correlation analysis of A β protein level measurements and AD biomarker levels.

Additional file 2: Fig. S1. A β peptide levels and *APP* and *PSEN1* expression in hippocampus and cortex of 5xFAD mice. **Fig. S2.** Analysis of A β aggregate formation using membrane filter assays and sucrose gradient centrifugations. **Fig. S3.** Analysis of wild-type expression profiles to assess whether the protein abundance changes detected in 5xFAD brains are more frequent among highly expressed mouse proteins. **Fig. S4.** Functional analysis of dysregulated proteins defined with a pairwise model in brains of 5xFAD mice. **Fig. S5.** Enrichment analysis of cell-type-specific marker proteins among dysregulated proteins in brains of 5xFAD mice. **Fig. S6.** IPA and gene ontology enrichment analysis of differentially expressed proteins defined with the full model in cortical and hippocampal tissues of 5xFAD mice. **Fig. S7.** Ingenuity pathway analysis of A β -correlated and anticorrelated DEPs defined by the pairwise model in brains of 5xFAD mice. **Fig. S8.** Numbers of pairwise common DEPs in the mouse datasets and datasets from human studies. **Fig. S9.** Strategy to define mouse protein signatures that are concordantly altered also in AD patient brains. **Fig. S10.** Investigation of the overlap of DEPs in brains of 5xFAD mice with DEPs in asymptomatic AD brains. **Fig. S11.** Analysis of the correlation in protein effect sizes between 5xFAD mouse and AD patient brains for proteins present in all studies. **Fig. S12.** Selection of the neuronal lysosome-associated protein A β by step-by-step data filtering. **Fig. S13.** Immunofluorescence analysis of 5xFAD brain slices. **Fig. S14.** Analysis of A β protein aggregates using human brain homogenates derived from AD patients and control individuals.

Additional file 3: Supplementary Excel File 1a. DEPs from 5xFAD versus wild-type tissue comparisons in hippocampus and cortex; DEPs were defined using the “pairwise model”; **Supplementary Excel File 1b.** Summary of the statistical calculations from **Supplementary Excel File 1a**; **Supplementary Excel File 1c.** DEPs in both hippocampal and cortical tissues defined through the “full model”; **Supplementary Excel File 2.** DEPs that correlate or anticorrelate to A β aggregate load in both hippocampal and cortical tissues defined through the “pairwise model”; **Supplementary Excel File 3.** Identified genes differentially down- or upregulated in cortex or hippocampus of 5xFAD mice; **Supplementary Excel File 4.** Results of the Ingenuity Pathway Analyses performed in **Figures 3g and 4e**; **Supplementary Excel File 5a.** Proteins with significant abundance changes from Johnson et al. 2020; **Supplementary Excel File 5b.** Proteins with significant abundance changes from Johnson et al. 2022; **Supplementary Excel File 5c.** Proteins with significant abundance changes from Johnson et al. 2022; **Supplementary Excel File 5d.** Proteins with significant abundance changes from Drummond et al. 2022; **Supplementary Excel File 6.** Numbers of common DEPs in mouse and human datasets; **Supplementary Excel File 7.** DEPs defined using a “pairwise model” and concomitantly altered both in mouse and human brain tissues from J20, J22 and D22. **Supplementary Excel File 8a.** The step-by-step selection process to identify the potential AD biomarker A β . **Supplementary Excel File 8b.** The top 25 A β -correlated proteins in mouse hippocampal tissues.

Acknowledgements

We thank Karola Bach, Stephanie Rode, Melanie Humpenöder (MDC Berlin), and Pascal Eede (Charité Berlin) for technical support. We are grateful to the genomics core facility (MDC Berlin) for sequencing RNAs. We thank Lidia Mateo and Patrick Aloy (IRB Barcelona) for providing assistance in data analyses and Thomas Willnow und Anne-Sophie Carlo-Spiewok (MDC Berlin) for providing us breeder pairs of the 5xFAD mouse model. Human brain samples for this study were provided by the Newcastle Brain Tissue Resource which is funded in part by a grant from the UK Medical Research Council (G0400074), by NIHR Newcastle Biomedical Research Centre awarded to the Newcastle upon Tyne NHS Foundation Trust and Newcastle University, and as part of the Brains for Dementia Research Program jointly funded by Alzheimer’s Research UK and Alzheimer’s Society.

Authors’ contributions

AB, NN, MK, PS, IB, AS, MZ, CS, LSS, ARW, and MR performed the experiments including mass spectrometry and microscopy imaging. AB, CH, EB, AI, ARW, MR, CMM, GD, and DB analyzed the data and designed specific experiments. MK, LMB, EJW, JEN, GD, BK, and OP provided reagents or technologies. The manuscript was written by EEW with support from AB, CH, and SS. EEW acquired the funding and provided overall supervision. All authors contributed to the conception of the study, and read and approved the final manuscript.

Funding

Open Access funding enabled and organized by Projekt DEAL. This study received funding from the Berlin Institute of Health (BIH) Collaborative Research grant “Elucidating the Proteostasis Network to Control Alzheimer’s Disease” funded by the German Federal Ministry for Education and Research (BMBF) to EEW and OP, the ERA-NET NEURON initiative, funded by the BMBF, grant no. 01W1301 ABETA ID, the Helmholtz Validation Fund grant no. HVF-0013 funded by the Helmholtz Association, Germany, (to EEW), and the Max Delbrück Center for Molecular Medicine in the Helmholtz Association for application-oriented research (to EEW). LMB holds fellowship and grant funding from the Huntington’s Disease Society of America, the Hereditary Disease Foundation, F. Hoffmann-La Roche AG, CHDI Foundation Inc, GSK and Medical Research Council UK. EJW reports grants from Medical Research Council UK, CHDI Foundation Inc, European Huntington’s Disease Network, and F. Hoffmann-La Roche Ltd. The Newcastle Brain Tissue Resource is funded in part by a grant from the UK Medical Research Council (G0400074), by NIHR Newcastle Biomedical Research Centre and Unit awarded to the Newcastle upon Tyne NHS Foundation Trust and Newcastle University, and as part of the Brains for Dementia Research Programme jointly funded by Alzheimer’s Research UK and Alzheimer’s Society.

Availability of data and materials

The RNA-seq data have been deposited in the Gene Expression Omnibus (GEO, [107]) database with the identifier GSE198226. (<https://www.ncbi.nlm.nih.gov/geo/query/acc.cgi?acc=GSE198226>) [108]. Raw sequencing reads are available from NCBI SRA PRJNA814239 (<https://www.ncbi.nlm.nih.gov/bioproject/PRJNA814239>). The mass spectrometry proteomics data have been deposited in the ProteomeXchange Consortium via the PRIDE [109] partner repository with the dataset identifier PXD030348 [110] and are available using the username: reviewer_pxd030348@ebi.ac.uk and the password: 8Hpbp7JG (<https://www.ebi.ac.uk/pride/login>).

Declarations

Ethics approval and consent to participate

All experiments using human data or samples were performed in accordance with the Declaration of Helsinki and approved by Charité University Medicine ethics committee (EA2/118/15), University College London (UCL)/UCL Hospitals Joint Research Ethics Committee and the Ethics Committee of the Capital Region of Denmark (H2-2011-085). Human brain tissue samples for this study were provided by the Newcastle Brain Tissue Resource (NBTR), Newcastle University, UK. All subjects gave written informed consent. Animal care was in accordance with the directive 2010/63/EU. The MDC has signed the Basel Declaration in 2012 and observes an internal animal welfare directive. Experimental procedures were approved by the local animal welfare authority in Berlin, Germany, under license number TVW G0073/17.

Consent for publication

Not applicable.

Competing interests

LMB reports personal fees from Hoffman La Roche Ltd, Remix Therapeutics, Annexon Biosciences, and Genentech. EJW reports personal fees from Hoffman La Roche Ltd, Triplet Therapeutics, PTC Therapeutics, Takeda, Teitur Trophics and Vico Therapeutics. All honoraria for these consultancies were paid through the offices of UCL Consultants Ltd., a wholly-owned subsidiary of University College London. The mentioned commercial entities have not participated in the design, performance, evaluation, or writing of the study. The remaining authors declare that they have no competing interests.

Author details

¹Neuroproteomics, Max Delbrück Center for Molecular Medicine in the Helmholtz Association, Robert-Rössle-Straße 10, 13125 Berlin, Germany. ²Core Unit Bioinformatics, Berlin Institute of Health at Charité - University Medicine Berlin, Charitéplatz 1, 10117 Berlin, Germany. ³Core Unit Proteomics, Berlin Institute of Health at Charité - University Medicine Berlin, Lindenberger Weg 80, 13125 Berlin, Germany. ⁴Advanced Light Microscopy, Max Delbrück Center for Molecular Medicine in the Helmholtz Association, Robert-Rössle-Straße 10, 13125 Berlin, Germany. ⁵Systems Biology of Gene Regulatory Elements, Max Delbrück Center for Molecular Medicine in the Helmholtz Association, Robert-Rössle-Straße 10, 13125 Berlin, Germany. ⁶Department of Psychiatry, Charité - University Medicine Berlin, Hindenburgdamm 30, 12203 Berlin, Germany. ⁷UCL Huntington's Disease Centre, UCL Queen Square Institute of Neurology, Queen Square, London WC1N 3BG, UK. ⁸National Hospital for Neurology & Neurosurgery, Queen Square, London WC1N 3BG, UK. ⁹Neurogenetics Clinic & Research Lab, Danish Dementia Research Centre, Rigshospitalet, University of Copenhagen, Section 8008, Inge Lehmanns Vej 8, 2100 Copenhagen, Denmark. ¹⁰Proteomics of Cellular Signalling, Luxembourg Institute of Health, 1a Rue Thomas Edison, 1445 Strassen, Luxembourg. ¹¹German Center for Neurodegenerative Diseases (DZNE), Charitéplatz 1, 10117 Berlin, Germany.

Received: 14 March 2022 Accepted: 22 June 2023

Published online: 20 July 2023

References

- Theuns J, Van Broeckhoven C. Genes for Alzheimer dementia *Acta neuropsychiatrica*. 1999;11:60–2.
- Bateman RJ, Xiong C, Benzinger TL, Fagan AM, Goate A, Fox NC, Marcus DS, Cairns NJ, Xie X, Blazey TM, et al. Clinical and biomarker changes in dominantly inherited Alzheimer's disease. *N Engl J Med*. 2012;367:795–804.
- Masters CL, Bateman R, Blennow K, Rowe CC, Sperling RA, Cummings JL. Alzheimer's disease. *Nat Rev Dis Primers*. 2015;1:15056.
- Zhu XC, Tan L, Wang HF, Jiang T, Cao L, Wang C, Wang J, Tan CC, Meng XF, Yu JT. Rate of early onset Alzheimer's disease: a systematic review and meta-analysis. *Ann Transl Med*. 2015;3:38.
- Rahman MM, Lendel C. Extracellular protein components of amyloid plaques and their roles in Alzheimer's disease pathology. *Mol Neurodegener*. 2021;16:59.
- Hyman BT, Phelps CH, Beach TG, Bigio EH, Cairns NJ, Carrillo MC, Dickson DW, Duyckaerts C, Frosch MP, Masliah E, et al. National Institute on Aging-Alzheimer's Association guidelines for the neuropathologic assessment of Alzheimer's disease. *Alzheimers Dementia*. 2012;8:1–13.
- De Strooper B, Saftig P, Craessaerts K, Vanderstichele H, Guhde G, Annaert W, Von Figura K, Van Leuven F. Deficiency of presenilin-1 inhibits the normal cleavage of amyloid precursor protein. *Nature*. 1998;391:387–90.
- Haass C, Kaether C, Thinakaran G, Sisodia S. Trafficking and proteolytic processing of APP. *Cold Spring Harb Perspect Med*. 2012;2:a006270.
- Hardy JA, Higgins GA. Alzheimer's disease: the amyloid cascade hypothesis. *Science*. 1992;256:184–5.
- Selkoe DJ. The molecular pathology of Alzheimer's disease. *Neuron*. 1991;6:487–98.
- Ricciarelli R, Fedele E. The amyloid cascade hypothesis in Alzheimer's disease: it's time to change our mind. *Curr Neuropharmacol*. 2017;15:926–35.
- Masters CL, Simms G, Weinman NA, Multhaup G, McDonald BL, Beyreuther K. Amyloid plaque core protein in Alzheimer disease and Down syndrome. *Proc Natl Acad Sci U S A*. 1985;82:4245–9.
- Blennow K, de Leon MJ, Zetterberg H. Alzheimer's disease. *Lancet*. 2006;368:387–403.
- Baranello RJ, Bharani KL, Padmaraju V, Chopra N, Lahiri DK, Greig NH, Pappolla MA, Sambamurti K. Amyloid-beta protein clearance and degradation (ABCD) pathways and their role in Alzheimer's disease. *Curr Alzheimer Res*. 2015;12:32–46.
- Andersen OM, Rudolph IM, Willnow TE. Risk factor SORL1: from genetic association to functional validation in Alzheimer's disease. *Acta Neuropathol*. 2016;132:653–65.
- Xu W, Tan L, Yu JT. The role of PICALM in Alzheimer's disease. *Mol Neurobiol*. 2015;52:399–413.
- Yamazaki Y, Zhao N, Caulfield TR, Liu CC, Bu G. Apolipoprotein E and Alzheimer disease: pathobiology and targeting strategies. *Nat Rev Neurol*. 2019;15:501–18.
- Shankar GM, Li S, Mehta TH, Garcia-Munoz A, Shepardson NE, Smith I, Brett FM, Farrell MA, Rowan MJ, Lemere CA, et al. Amyloid-beta protein dimers isolated directly from Alzheimer's brains impair synaptic plasticity and memory. *Nat Med*. 2008;14:837–42.
- Sorrentino V, Romani M, Mouchiroud L, Beck JS, Zhang H, D'Amico D, Moullan N, Potenza F, Schmid AW, Rietsch S, et al. Enhancing mitochondrial proteostasis reduces amyloid-beta proteotoxicity. *Nature*. 2017;552:187–93.
- Landel V, Baranger K, Virard I, Loriod B, Khrestchatsky M, Rivera S, Benech P, Feron F. Temporal gene profiling of the 5xFAD transgenic mouse model highlights the importance of microglial activation in Alzheimer's disease. *Mol Neurodegener*. 2014;9:33.
- Oakley H, Cole SL, Logan S, Maus E, Shao P, Craft J, Guillozet-Bongaarts A, Ohno M, Disterhoft J, Van Eldik L, et al. Intraneuronal beta-amyloid aggregates, neurodegeneration, and neuron loss in transgenic mice with five familial Alzheimer's disease mutations: potential factors in amyloid plaque formation. *J Neurosci*. 2006;26:10129–40.
- Gatt A, Whitfield DR, Ballard C, Doherty P, Williams G. Alzheimer's disease progression in the 5xFAD mouse captured with a multiplex gene expression array. *J Alzheimers Dis*. 2019;72:1177–91.
- Hong I, Kang T, Yoo Y, Park R, Lee J, Lee S, Kim J, Song B, Kim SY, Moon M, et al. Quantitative proteomic analysis of the hippocampus in the 5xFAD mouse model at early stages of Alzheimer's disease pathology. *J Alzheimers Dis*. 2013;36:321–34.
- Zhou Y, Song WM, Andhey PS, Swain A, Levy T, Miller KR, Poliani PL, Cominelli M, Grover S, Gilfillan S, et al. Human and mouse single-nucleus transcriptomics reveal TREM2-dependent and TREM2-independent cellular responses in Alzheimer's disease. *Nat Med*. 2020;26:131–42.
- Bai B, Wang X, Li Y, Chen PC, Yu K, Dey KK, Yarbro JM, Han X, Lutz BM, Rao S, et al. Deep multilayer brain proteomics identifies molecular networks in Alzheimer's disease progression. *Neuron*. 2020;105(975–991): e977.
- Liu P, Reichl JH, Rao ER, McNellis BM, Huang ES, Hemmy LS, Forster CL, Kuskowski MA, Borchelt DR, Vassar R, et al. Quantitative comparison of dense-core amyloid plaque accumulation in amyloid-beta protein precursor transgenic mice. *J Alzheimers Dis*. 2017;56:743–61.
- Bundy JL, Vied C, Badger C, Nowakowski RS. Sex-biased hippocampal pathology in the 5xFAD mouse model of Alzheimer's disease: a multi-omic analysis. *J Comp Neurol*. 2019;527:462–75.
- Kim DK, Han D, Park J, Choi H, Park JC, Cha MY, Woo J, Byun MS, Lee DY, Kim Y, Mook-Jung I. Deep proteome profiling of the hippocampus in the 5xFAD mouse model reveals biological process alterations and a novel biomarker of Alzheimer's disease. *Exp Mol Med*. 2019;51:1–17.
- Farfel-Becker T, Roney JC, Cheng XT, Li S, Cuddy SR, Sheng ZH. Neuronal soma-derived degradative lysosomes are continuously delivered to distal axons to maintain local degradation capacity. *Cell Rep*. 2019;28(51–64): e54.
- Boeddrich A, Babila JT, Wiglenda T, Diez L, Jacob M, Nietfeld W, Huska MR, Haenig C, Groenke N, Buntru A, et al. The anti-amyloid compound DO1 decreases plaque pathology and neuroinflammation-related expression changes in 5xFAD transgenic mice. *Cell Chem Biol*. 2019;26(109–120): e107.
- Schipke CG, De Vos A, Fuentes M, Jacobs D, Vanmechelen E, Peters O. Neurogranin and BACE1 in CSF as potential biomarkers differentiating

- depression with cognitive deficits from early Alzheimer's disease: a pilot study. *Dementia and geriatric cognitive disorders extra*. 2018;8:277–89.
32. Schipke CG, Prokop S, Heppner FL, Heuser I, Peters O. Comparison of immunosorbent assays for the quantification of biomarkers for Alzheimer's disease in human cerebrospinal fluid. *Dement Geriatr Cogn Disord*. 2011;31:139–45.
 33. Vinther-Jensen T, Simonsen AH, Budtz-Jorgensen E, Hjerminde LE, Nielsen JE. Ubiquitin: a potential cerebrospinal fluid progression marker in Huntington's disease. *Eur J Neurol*. 2015;22:1378–84.
 34. Rodrigues FB, Byrne L, McColgan P, Robertson N, Tabrizi SJ, Leavitt BR, Zetterberg H, Wild EJ. Cerebrospinal fluid total tau concentration predicts clinical phenotype in Huntington's disease. *J Neurochem*. 2016;139:22–5.
 35. Wild EJ, Boggio R, Langbehn D, Robertson N, Haider S, Miller JR, Zetterberg H, Leavitt BR, Kuhn R, Tabrizi SJ, et al. Quantification of mutant huntingtin protein in cerebrospinal fluid from Huntington's disease patients. *J Clin Invest*. 2015;125:1979–86.
 36. Braak H, Braak E. Neuropathological staging of Alzheimer-related changes. *Acta Neuropathol*. 1991;82:239–59.
 37. Braak H, Alafuzoff I, Arzberger T, Kretschmar H, Del Tredici K. Staging of Alzheimer disease-associated neurofibrillary pathology using paraffin sections and immunocytochemistry. *Acta Neuropathol*. 2006;112:389–404.
 38. Haenig C, Atias N, Taylor AK, Mazza A, Schaefer MH, Russ J, Riechers SP, Jain S, Coughlin M, Fontaine JF, et al. Interactome Mapping Provides a Network of Neurodegenerative Disease Proteins and Uncovers Widespread Protein Aggregation in Affected Brains. *Cell Rep*. 2020;32: 108050.
 39. Paxinos G, Franklin KBJ. The mouse brain in stereotaxic coordinates. Academic Press; 2001.
 40. Rappsilber J, Ishihama Y, Mann M. Stop and go extraction tips for matrix-assisted laser desorption/ionization, nano-electrospray, and LC/MS sample pretreatment in proteomics. *Anal Chem*. 2003;75:663–70.
 41. Johnson ECB, Dammer EB, Duong DM, Ping L, Zhou M, Yin L, Higginbotham LA, Guajardo A, White B, Troncoso JC, et al. Large-scale proteomic analysis of Alzheimer's disease brain and cerebrospinal fluid reveals early changes in energy metabolism associated with microglia and astrocyte activation. *Nat Med*. 2020;26:769–80.
 42. Johnson ECB, Carter EK, Dammer EB, Duong DM, Gerasimov ES, Liu Y, Liu J, Betarbet R, Ping L, Yin L, et al. Large-scale deep multi-layer analysis of Alzheimer's disease brain reveals strong proteomic disease-related changes not observed at the RNA level. *Nat Neurosci*. 2022;25(2):213–225.
 43. Drummond E, Kavanagh T, Pires G, Marta-Ariza M, Kanshin E, Nayak S, Faustin A, Berdah V, Ueberheide B, Wisniewski T. The amyloid plaque proteome in early onset Alzheimer's disease and Down syndrome. *Acta Neuropathol Commun*. 2022;10:53.
 44. Dobin A, Davis CA, Schlesinger F, Drenkow J, Zaleski C, Jha S, Batut P, Chaisson M, Gingeras TR. STAR: ultrafast universal RNA-seq aligner. *Bioinformatics*. 2013;29:15–21.
 45. Frankish A, Diekhans M, Jungreis I, Lagarde J, Loveland JE, Mudge JM, Sisu C, Wright JC, Armstrong J, Barnes I, et al. GENCODE 2021. *Nucleic Acids Res*. 2021;49:D916–23.
 46. Love MI, Huber W, Anders S. Moderated estimation of fold change and dispersion for RNA-seq data with DESeq2. *Genome Biol*. 2014;15:550.
 47. Bult CJ, Blake JA, Smith CL, Kadin JA, Richardson JE. Mouse Genome Database G: Mouse Genome Database (MGD) 2019. *Nucleic Acids Res*. 2019;47:D801–6.
 48. Howe KL, Achuthan P, Allen J, Allen J, Alvarez-Jarreta J, Amodè MR, Armean IM, Azov AG, Bennett R, Bhai J, et al. Ensembl 2021. *Nucleic Acids Res*. 2021;49:D884–91.
 49. Sharma K, Schmitt S, Bergner CG, Tyanova S, Kannaiyan N, Manrique-Hoyos N, Kongi K, Cantuti L, Hanisch UK, Phillips MA, et al. Cell type- and brain region-resolved mouse brain proteome. *Nat Neurosci*. 2015;18:1819–31.
 50. Marzocco AM, Flotemeyer M, Buhler A, Obermuller U, Staufienbiel M, Jucker M, Baumann F. Highly potent intracellular membrane-associated Abeta seeds. *Sci Rep*. 2016;6:28125.
 51. Kramer A, Green J, Pollard J Jr, Tugendreich S. Causal analysis approaches in ingenuity pathway analysis. *Bioinformatics*. 2014;30:523–30.
 52. Eden E, Navon R, Steinfeld I, Lipson D, Yakhini Z. GOrilla: a tool for discovery and visualization of enriched GO terms in ranked gene lists. *BMC Bioinformatics*. 2009;10:48.
 53. Youmans KL, Leung S, Zhang J, Maus E, Baysac K, Bu G, Vassar R, Yu C, LaDu MJ. Amyloid-beta42 alters apolipoprotein E solubility in brains of mice with five familial AD mutations. *J Neurosci Methods*. 2011;196:51–9.
 54. Wanker EE, Scherzinger E, Heiser V, Sittler A, Eickhoff H, Leirach H. Membrane filter assay for detection of amyloid-like polyglutamine-containing protein aggregates. *Methods Enzymol*. 1999;309:375–86.
 55. McLellan ME, Kajdasz ST, Hyman BT, Bacskai BJ. In vivo imaging of reactive oxygen species specifically associated with thioflavine S-positive amyloid plaques by multiphoton microscopy. *J Neurosci*. 2003;23:2212–7.
 56. Cox J, Matic I, Hilger M, Nagaraj N, Selbach M, Olsen JV, Mann M. A practical guide to the MaxQuant computational platform for SILAC-based quantitative proteomics. *Nat Protoc*. 2009;4:698–705.
 57. Swerdlow RH. Mitochondria and Mitochondrial Cascades in Alzheimer's disease. *J Alzheimers Dis*. 2018;62:1403–16.
 58. Nader N, Ng SS, Wang Y, Abel BS, Chrousos GP, Kino T. Liver x receptors regulate the transcriptional activity of the glucocorticoid receptor: implications for the carbohydrate metabolism. *PLoS ONE*. 2012;7: e26751.
 59. Laffitte BA, Repa JJ, Joseph SB, Wilpitz DC, Kast HR, Mangelsdorf DJ, Tontonoz P. LXRs control lipid-inducible expression of the apolipoprotein E gene in macrophages and adipocytes. *Proc Natl Acad Sci U S A*. 2001;98:507–12.
 60. Johnson SA, Lampert-Etchells M, Pasinetti GM, Rozovsky I, Finch CE. Complement mRNA in the mammalian brain: responses to Alzheimer's disease and experimental brain lesioning. *Neurobiol Aging*. 1992;13:641–8.
 61. Hong S, Beja-Glasser VF, Nfonoyim BM, Frouin A, Li S, Ramakrishnan S, Merry KM, Shi Q, Rosenthal A, Barres BA, et al. Complement and microglia mediate early synapse loss in Alzheimer mouse models. *Science*. 2016;352:712–6.
 62. Keilani S, Lun Y, Stevens AC, Williams HN, Sjoberg ER, Khanna R, Valenzano KJ, Checler F, Buxbaum JD, Yanagisawa K, et al. Lysosomal dysfunction in a mouse model of Sandhoff disease leads to accumulation of ganglioside-bound amyloid-beta peptide. *J Neurosci*. 2012;32:5223–36.
 63. Lathe R, Sapronova A, Kotelevtsev Y. Atherosclerosis and Alzheimer-diseases with a common cause? Inflammation, oxysterols, vasculature. *BMC Geriatr*. 2014;14:36.
 64. Abella JV, Galloni C, Pernier J, Barry DJ, Kjaer S, Carlier MF, Way M. Isoform diversity in the Arp2/3 complex determines actin filament dynamics. *Nat Cell Biol*. 2016;18:76–86.
 65. Henriques AG, Oliveira JM, Carvalho LP, da Cruz ESOAB: Abeta influences cytoskeletal signaling cascades with consequences to Alzheimer's disease. *Mol Neurobiol*. 2015;52:1391–1407.
 66. Kommaddi RP, Tomar DS, Karunakaran S, Bapat D, Nanguneri S, Ray A, Schneider BL, Nair D, Ravindranath V. Glutaredoxin1 diminishes amyloid beta-mediated oxidation of F-Actin and reverses cognitive deficits in an Alzheimer's disease mouse model. *Antioxid Redox Signal*. 2019;31:1321–38.
 67. Wang Z, Jackson RJ, Hong W, Taylor WM, Corbett GT, Moreno A, Liu W, Li S, Frosch MP, Slutsky I, et al. Human brain-derived Abeta oligomers bind to synapses and disrupt synaptic activity in a manner that requires APP. *J Neurosci*. 2017;37:11947–66.
 68. Jack CR Jr, Bennett DA, Blennow K, Carrillo MC, Dunn B, Haeberlein SB, Holtzman DM, Jagust W, Jessen F, Karlawish J, et al. NIA-AA Research Framework: toward a biological definition of Alzheimer's disease. *Alzheimers Dementia*. 2018;14:535–62.
 69. de Wilde MC, Overk CR, Sijben JW, Masliah E. Meta-analysis of synaptic pathology in Alzheimer's disease reveals selective molecular vesicular machinery vulnerability. *Alzheimers Dementia*. 2016;12:633–44.
 70. Ihara Y, Morishima-Kawashima M, Nixon R. The ubiquitin-proteasome system and the autophagic-lysosomal system in Alzheimer disease. *Cold Spring Harb Perspect Med*. 2012;2(8):a006361.
 71. Knopman DS, Amieva H, Petersen RC, Chetelat G, Holtzman DM, Hyman BT, Nixon RA, Jones DT. Alzheimer disease. *Nat Rev Dis Primers*. 2021;7:33.
 72. Keren-Kaplan T, Bonifacino JS. ARL8 Relieves SKIP autoinhibition to enable coupling of lysosomes to Kinesin-1. *Curr Biol*. 2021;31(540–554): e545.
 73. Pu J, Schindler C, Jia R, Jarnik M, Backlund P, Bonifacino JS. BORC, a multisubunit complex that regulates lysosome positioning. *Dev Cell*. 2015;33:176–88.

74. Eskelinen EL. Roles of LAMP-1 and LAMP-2 in lysosome biogenesis and autophagy. *Mol Aspects Med.* 2006;27:495–502.
75. Krance SH, Wu CY, Chan ACY, Kwong S, Song BX, Xiong LY, Ouk M, Chen MH, Zhang J, Yung A, et al. Endosomal-lysosomal and autophagy pathway in Alzheimer's disease: a systematic review and meta-analysis. *J Alzheimers Dis.* 2022;88:1279–92.
76. Armstrong A, Mattsson N, Appelqvist H, Janefjord C, Sandin L, Agholme L, Olsson B, Svensson S, Blennow K, Zetterberg H, Kagedal K. Lysosomal network proteins as potential novel CSF biomarkers for Alzheimer's disease. *Neuromolecular Med.* 2014;16:150–60.
77. Gowrishankar S, Yuan P, Wu Y, Schrag M, Paradise S, Grutzendler J, De Camilli P, Ferguson SM. Massive accumulation of luminal protease-deficient axonal lysosomes at Alzheimer's disease amyloid plaques. *Proc Natl Acad Sci U S A.* 2015;112:E3699–3708.
78. Busche MA, Hyman BT. Synergy between amyloid-beta and tau in Alzheimer's disease. *Nat Neurosci.* 2020;23:1183–93.
79. Long JM, Holtzman DM. Alzheimer disease: an update on pathobiology and treatment strategies. *Cell.* 2019;179:312–39.
80. Nelson PT, Alafuzoff I, Bigio EH, Bouras C, Braak H, Cairns NJ, Castellani RJ, Crain BJ, Davies P, Del Tredici K, et al. Correlation of Alzheimer disease neuropathologic changes with cognitive status: a review of the literature. *J Neuropathol Exp Neurol.* 2012;71:362–81.
81. Buee L, Bussiere T, Buee-Scherrer V, Delacourte A, Hof PR. Tau protein isoforms, phosphorylation and role in neurodegenerative disorders. *Brain Res Brain Res Rev.* 2000;33:95–130.
82. Sato C, Barthelemy NR, Mawuenyega KG, Patterson BW, Gordon BA, Jockel-Balsarotti J, Sullivan M, Crisp MJ, Kasten T, Kirmess KM, et al. Tau kinetics in neurons and the human central nervous system. *Neuron.* 2018;97(1284–1298): e1287.
83. Keren-Shaul H, Spinrad A, Weiner A, Matcovitch-Natan O, Dvir-Szternfeld R, Ulland TK, David E, Baruch K, Lara-Astaiso D, Toth B, et al. A unique microglia type associated with restricting development of Alzheimer's disease. *Cell.* 2017;169(1276–1290): e1217.
84. Sevigny J, Chiao P, Bussiere T, Weinreb PH, Williams L, Maier M, Dunstan R, Salloway S, Chen T, Ling Y, et al. The antibody aducanumab reduces Aβ plaques in Alzheimer's disease. *Nature.* 2016;537:50–6.
85. Wang H, Dey KK, Chen PC, Li Y, Niu M, Cho JH, Wang X, Bai B, Jiao Y, Chepyala SR, et al. Integrated analysis of ultra-deep proteomes in cortex, cerebrospinal fluid and serum reveals a mitochondrial signature in Alzheimer's disease. *Mol Neurodegener.* 2020;15:43.
86. Cenini G, Voos W. Mitochondria as potential targets in Alzheimer disease therapy: an update. *Front Pharmacol.* 2019;10:902.
87. Wingo AP, Dammer EB, Breen MS, Logsdon BA, Duong DM, Troncosco JC, Thambisetty M, Beach TG, Serrano GE, Reiman EM, et al. Large-scale proteomic analysis of human brain identifies proteins associated with cognitive trajectory in advanced age. *Nat Commun.* 2019;10:1619.
88. Hosp F, Vossfeldt H, Heinig M, Vasiljevic D, Arumughan A, Wyler E, Landthaler M, Hubner N, Wanker EE, Lannfelt L, et al. Quantitative interaction proteomics of neurodegenerative disease proteins. *Cell Rep.* 2015;11:1134–46.
89. Pera M, Larrea D, Guardia-Laguarta C, Montesinos J, Velasco KR, Agrawal RR, Xu Y, Chan RB, Di Paolo G, Mehler MF, et al. Increased localization of APP-C99 in mitochondria-associated ER membranes causes mitochondrial dysfunction in Alzheimer disease. *Embo J.* 2017;36:3356–71.
90. Briston T, Hicks AR. Mitochondrial dysfunction and neurodegenerative proteinopathies: mechanisms and prospects for therapeutic intervention. *Biochem Soc Trans.* 2018;46:829–42.
91. Chen WT, Lu A, Craessaerts K, Pavie B, Sala Frigerio C, Corthout N, Qian X, Lalakova J, Kuhnemund M, Voytyuk I, et al. Spatial transcriptomics and in situ sequencing to study Alzheimer's disease. *Cell.* 2020;182(976–991): e919.
92. Tonnie E, Trushina E. Oxidative stress, synaptic dysfunction, and Alzheimer's disease. *J Alzheimers Dis.* 2017;57:1105–21.
93. De Pace R, Britt DJ, Mercurio J, Foster AM, Djavaherian L, Hoffmann V, Abebe D, Bonifacio JS. Synaptic vesicle precursors and lysosomes are transported by different mechanisms in the axon of mammalian neurons. *Cell Rep.* 2020;31: 107775.
94. Klassen MP, Wu YE, Maeder CI, Nakae I, Cueva JG, Lehrman EK, Tada M, Gengyo-Ando K, Wang GJ, Goodman M, et al. An Arf-like small G protein, ARL-8, promotes the axonal transport of presynaptic cargoes by suppressing vesicle aggregation. *Neuron.* 2010;66:710–23.
95. Vukoja A, Rey U, Petzoldt AG, Ott C, Vollweider D, Quentin C, Puchkov D, Reynolds E, Lehmann M, Hohensee S, et al. Presynaptic biogenesis requires axonal transport of lysosome-related vesicles. *Neuron.* 2018;99(1216–1232): e1217.
96. Griffin EF, Yan X, Caldwell KA, Caldwell GA. Distinct functional roles of Vps41-mediated neuroprotection in Alzheimer's and Parkinson's disease models of neurodegeneration. *Hum Mol Genet.* 2018;27:4176–93.
97. Roney JC, Li S, Farfel-Becker T, Huang N, Sun T, Xie Y, Cheng XT, Lin MY, Platt FM, Sheng ZH. Lipid-mediated motor-adaptor sequestration impairs axonal lysosome delivery leading to autophagic stress and dystrophy in Niemann-Pick type C. *Dev Cell.* 2021;56(1452–1468): e1458.
98. Annunziata I, Patterson A, Helton D, Hu H, Moshiah S, Gomerio E, Nixon R, d'Azzo A. Lysosomal NEU1 deficiency affects amyloid precursor protein levels and amyloid-beta secretion via deregulated lysosomal exocytosis. *Nat Commun.* 2013;4:2734.
99. Siman R, Mistretta S, Durkin JT, Savage MJ, Loh T, Trusko S, Scott RW. Processing of the beta-amyloid precursor. Multiple proteases generate and degrade potentially amyloidogenic fragments. *J Biol Chem.* 1993;268:16602–16609.
100. Cataldo AM, Paskevich PA, Kominami E, Nixon RA. Lysosomal hydrolases of different classes are abnormally distributed in brains of patients with Alzheimer disease. *Proc Natl Acad Sci U S A.* 1991;88:10998–1002.
101. Zhang L, Sheng R, Qin Z. The lysosome and neurodegenerative diseases. *Acta Biochim Biophys Sin (Shanghai).* 2009;41:437–45.
102. Bai B, Vanderwall D, Li Y, Wang X, Poudel S, Wang H, Dey KK, Chen PC, Yang K, Peng J. Proteomic landscape of Alzheimer's disease: novel insights into pathogenesis and biomarker discovery. *Mol Neurodegener.* 2021;16:55.
103. Bader JM, Geyer PE, Muller JB, Strauss MT, Koch M, Leyboldt F, Koertvelyessy P, Bittner D, Schipke CG, Incesoy EI, et al. Proteome profiling in cerebrospinal fluid reveals novel biomarkers of Alzheimer's disease. *Mol Syst Biol.* 2020;16: e9356.
104. Higginbotham L, Ping L, Dammer EB, Duong DM, Zhou M, Gearing M, Hurst C, Glass JD, Factor SA, Johnson ECB, et al. Integrated proteomics reveals brain-based cerebrospinal fluid biomarkers in asymptomatic and symptomatic Alzheimer's disease. *Sci Adv.* 2020;6(43): eaa29360.
105. Kvartsberg H, Duits FH, Ingelsson M, Andreasen N, Ohrfelt A, Andersson K, Brinkmalm G, Lannfelt L, Minthon L, Hansson O, et al. Cerebrospinal fluid levels of the synaptic protein neurogranin correlates with cognitive decline in prodromal Alzheimer's disease. *Alzheimers Dementia.* 2015;11:1180–90.
106. Preische O, Schultz SA, Apel A, Kuhle J, Kaeser SA, Barro C, Graber S, Kuder-Buletta E, LaFougere C, Laske C, et al. Serum neurofilament dynamics predicts neurodegeneration and clinical progression in presymptomatic Alzheimer's disease. *Nat Med.* 2019;25:277–83.
107. Barrett T, Wilhite SE, Ledoux P, Evangelista C, Kim IF, Tomashevsky M, Marshall KA, Phillippy KH, Sherman PM, Holko M, et al. NCBI GEO: archive for functional genomics data sets—update. *Nucleic Acids Res.* 2013;41:D991–995.
108. Suenkel C, Rybak-Wolf A, Ivanov A, Blanc E, Boeddrich A, Haenig C, Wanker EE. A proteomics analysis of 5xFAD mouse brain regions reveals the lysosome-associated protein Arl8b as a candidate biomarker for Alzheimer's disease. *GSE198226, Gene Expression Omnibus.* 2023. <https://www.ncbi.nlm.nih.gov/geo/query/acc.cgi?acc=GSE198226>.
109. Perez-Riverol Y, Csordas A, Bai J, Bernal-Llinares M, Hewapathirana S, Kundu DJ, Inuganti A, Griss J, Mayer G, Eisenacher M, et al. The PRIDE database and related tools and resources in 2019: improving support for quantification data. *Nucleic Acids Res.* 2019;47:D442–50.
110. Kirchner M, Blanc E, Boeddrich A, Haenig C, Beule D, Dittmar, G, Wanker EE. A proteomics analysis of 5xFAD mouse brain regions reveals the lysosome-associated protein Arl8b as a candidate biomarker for Alzheimer's disease. *PXD030348, ProteomeXchange, ProteomeCentral, PRIDE - Proteomics Identifications Database.* 2023. <https://proteomecentral.proteomexchange.org/cgi/GetDataset?ID=PXD030348>.

Publisher's Note

Springer Nature remains neutral with regard to jurisdictional claims in published maps and institutional affiliations.